FIGURING HIGH ASPHERIC MIRRORS BY ELASTIC DEFORMATION METHOD

by

YAN KANG
B.Sc., Xian Institute of Technology, 1982

A THESIS SUBMITTED IN PARTIAL FULFILLMENT
OF THE REQUIREMENTS FOR THE DEGREE OF

MASTER OF APPLIED SCIENCE

in the Department of
Mechanical Engineering

We accept this thesis as conforming
to the required standard

[redacted]

Dr. H. Richardson, Supervisor, Dept. of Mech. Eng.

[redacted]

Dr. B. Tabarrok, Supervisor, Chairman, Dept. of Mech. Eng.

[redacted]

Dr. S. Dost, Graduate Advisor, Dept. of Mech. Eng.

[redacted]

Dr. W-S. Lu, Outside Member, Dept. of Elect. & Comp. Eng.

[redacted]

Dr. G. B. Friedmann, External Examiner, Dept. of Phys. & Astr.

Supervisors: Dr. H. Richardson and Dr. B. Tabarrok

Abstract

Aspheric surfaces play an important role in optical systems[4], but the application of such surfaces is constrained due to difficulties of fabrication.

In this thesis, the feasibility of figuring aspheric surfaces is investigated using the elastic deformation techniques. Specifically, the primary mirror of the proposed Space Debris Telescope is researched. This mirror consists of a concave hyperboloid with a fast focal ratio of $f/0.66$ and has a conic constant of $k = -1.255$. The combination results in an exceptionally aspheric mirror make this mirror very difficult to produce.

In this thesis we present a general method for production of aspheric mirrors by elastic deformation. To do this a general function describing the deflection and orientation of aspheric surfaces is presented. This function can be used for most aspheres including a sphere. By means of the elastic plate theory, the load distributions can be found to produce the desired deformation.

Different finite element models are constructed to estimate the stresses in the mirror when the deflection is prescribed. The problem of determining an adequate number of discrete points for applying the forces and a best-fitting sphere for an aspheric surface are investigated. Stresses in the mirror are determined and checked to see that the chosen material has sufficient strength.

Examiners:

Dr. H. Richardson, Supervisor (Dept. of Mechanical Engineering)

Dr. B. Tabarrok, Supervisor, Chairman (Dept. of Mechanical Engineering)

Dr. S. Dost, Graduate Advisor (Dept. of Mechanical Engineering)

Dr. W-S. Lu, Outside Member (Dept. of Elect. & Comp. Eng.)

Dr. G. B. Friedmann, External Examiner (Dept. of Physics & Astronomy)

Acknowledgments

The author wishes to express his sincere gratitude and deep appreciation to:

Dr. H. Richardson for his conception of the present work and suggestions.

Dr. B. Tabarrok for his encouragement and support, for his contributions towards the implementation of this manuscript.

Dr. J. Haddow for useful discussions and advice during this research. Dr. G. Friedmann and Dr. S. Dost for their valuable comments.

Patricia Crane for graciously volunteering to read and comment on the thesis.

All friends of mine who encouraged me through difficult time.

To my parents and my daughter

Table of Contents

List of Figures

List of Tables

Chapter 1

Introduction

1.1 The Topic

The object of any engineering analysis is to predict the behaviour of a physical system. In order to realize this goal, one develops mathematical models of the physical system. The accuracy of predictions depends on the simplifying assumptions used in creating the mathematical model, the material properties and the geometric dimensions.

From the deflection of a plate which is a function of the two coordinates in the plane of the plate, one can determine all the stress components in the plate. Moreover, the loads required to produce the desired deflection will be determined by the elastic plate theory. Thus the deflection function gives all the necessary information for computing the loads and the stresses at any point in the plate.

In this thesis a mathematical model of an elastic plate deformation is used to simulate the behaviour of a mirror, namely the primary mirror of the proposed Space Debris Telescope (SDT) [27] in a practical manner, and it extends the analysis to a general case suitable for most aspheric mirrors.

The linear plate theory can yield very good results providing the physical system, namely the mirror, suffers small deflections.

To make the descriptions clear, the following terminology is defined as

follows[4]:

- Asphericity:

  The difference between a required surface and an osculating (or best fit) sphere.

- Focal ratio:

  The ratio of focal length to aperture of mirror.

- Conic constant(k):

  $k = -e^2$ (e is the eccentricity). The actual shape of conic mirror depends on the value of k.

The proposed SDT consists of three different mirrors, called the primary, secondary and tertiary, mirrors. The optical layout is shown in Fig.(1.1). The primary mirror is a pure conic and is the most aspheric. The secondary and tertiary mirrors have additional aspheric terms but are less aspheric. The primary mirror described in this thesis is a concave hyperboloid 1.6 meter in diameter and vertex radius of curvature of 2.111 meters. This mirror requires a fast focal ratio of $f/0.66$ and a conic constant of $k = -1.255$ which is 25.5 percent more aspheric than a paraboloid with the same focal ratio. The surface departs from the best-fitting-sphere by 1.6612 mm peak-to-valley−−about 17 times the asphericity of the fastest 4-meter classical mirror polished to date [22]. A moderately high surface accuracy for good image quality is also required by the mirror. This fast primary mirror offers great advantages of performance in the telescope, but it presents great difficulties in fabrication. As a rough guide, the difficulty of changing the deflection related to the different focal ratios and conic constants is expressed by a modified formula given by Martin et al [23]:

$$\Delta z \sim k\frac{D'}{4}(\frac{D'}{f})^3 \ (mm) \tag{1.1}$$

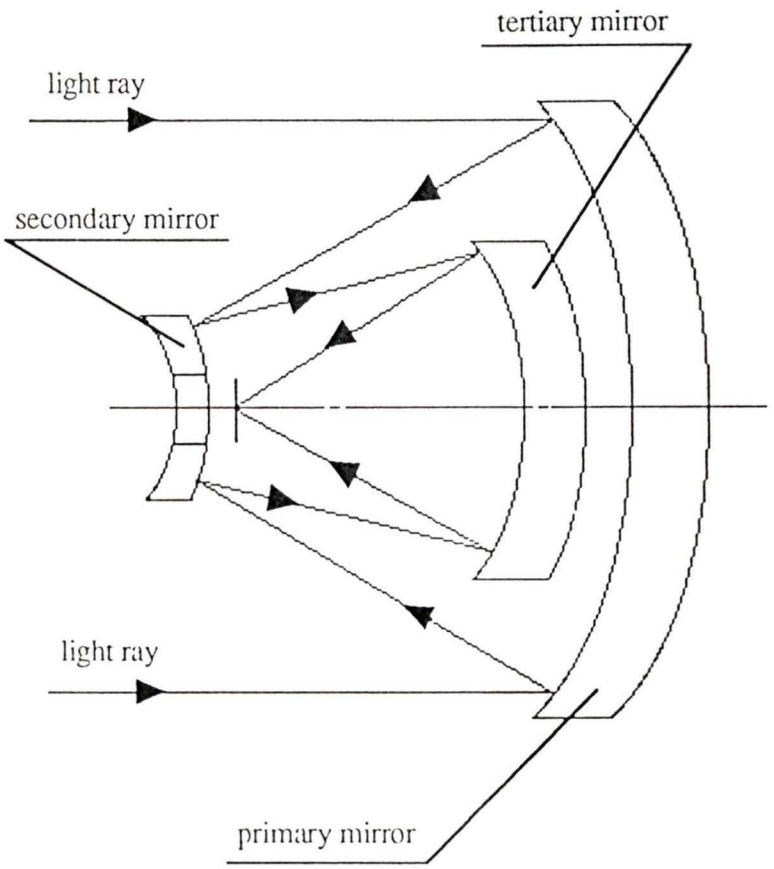

Figure 1.1: Sketch of optical system for Space Debris Telescope.

where D' is the diameter in meters, f/D' is the focal ratio and Δz is the magnitude of deflection.

The deflection changes rapidly with focal ratio and with conic constant as shown in Table 1.1. As the stress is proportional to the deflection and thickness of the mirror, high stresses induced by large deflection will rupture the glasses, or exceed the elastic limit of the materials used. Thus the proposed SDT mirror presents a serious challenge caused by its fast focal ratio and it is aspheric.

Table 1.1: Deflections as a function of the focal ratio and conic constant. Mirror diameter of D' is $1600mm$ and best-fitting spheres are used (unit: mm).

Focal ratio (f/D')	Deflection ($k = -1$)	Best fit sphere radius	Deflection ($k = -1.255$)	Best fit sphere radius
0.66	1.3237	2186.8	1.6612	2205.3
1.0	0.3903	3250.0	0.4856	3262.6
1.2	0.2252	3881.7	0.2817	3892.2
2.5	0.0250	8020.0	0.0313	8025.1

One way to manufacture an aspheric mirror is to use the elastic deformation methods which are both economical and practical.

The elastic deformation methods can be divided into the stressed lap and stressed mirror methods depending on whether the loads are applied on the lap or on the mirror blank.

In the stressed lap method, a set of forces is applied along the edge of the lap-disk to produce the necessary deflection. The lap moves over the entire mirror surface under computer control and actively changes its shape to match the aspheric surface.

In the stressed mirror method, a set of forces is applied along the edge of a mirror rather than the lap-disk. When the desired deflection is achieved, a sphere is used to grind and polish the mirror blank. After the forces are removed, the fabricated mirror elastically deforms into an asphere.

Among problems related to the elastic deformation methods, an important but little studied problem is how to describe a general deflection function which can deal with most aspheric surfaces rather than a special surface such as a paraboloid [11] [19] [22]. If such a deflection function can be generated, the necessary forces can be determined to achieve a desired deflection for the mirror using elastic deformation technique.

This thesis attempts to develop such a function. To obtain a desired deformation, it is convenient to apply forces at specified edge points, rather than on a continuous surface. Thus, in this thesis only edge forces are considered. We shall determine adequate points for the applied forces to obtain the desired deformation. The problem of determining the number of discrete points where forces are applied is solved by using the finite element method. The basic requirement for a viable technique is the need to obtain a specified accuracy of shape. Either the stressed lap or stressed mirror method satisfy these requirements. A desired accuracy can be achieved iteratively i.e. by polishing the mirror, measuring the results, modifying the applied forces, repolishing the mirror again and so on.

The stressed mirror method is suited to producing mirrors with small asphericity and slow focal ratios because glass is usually used as the mirror blank and cannot be stressed beyond a certain level. The stressed lap method is not limited by the same restriction if the proper geometric parameters of lap are chosen. The stressed lap and stressed mirror methods require that the deflection function describe the differences between an off-axis conic and an on-axis conic sections, and a conic and a spherical surface, respectively.

1.2 Review of Current Technologies

Fabricating techniques for aspheric surfaces have been studied since the beginning of the last century. The proposed methods can be divided into the following forms[7][8][22] [28]:

- Traditional method:
  This method requires many testing and polishing iterations with an experienced optician to calculate the required pitch pattern and polishing time at each step. It is difficult to use such a technique to produce an aspherical mirror with high quality, such as a mirror with a focal ratio of $f/0.66$.

- Computer-controlled polishing method:
  This method uses a very small lap and short polish strokes to control the surface shape by dwelling more or less on a spot, depending on whether the spot is low or high. This method will be slow for mirrors with fast focal ratios or large asphericity.

- Pressure controlled lap method:
  In this method the mirror surface is controlled by varying the pressure distribution across the lap. The figuring accuracy is maintained by using a flexible lap. Therefore, a large lap must be used. This technique is suited to mirrors with small deflections.

- Computer-controlled diamond turning method:
  This method uses a small diamond head as the lap to cut material from the substrate and figure an aspheric mirror, which is then aluminized. Thus this method is not limited by the asphericity or focal ratio of the mirror. The materials used for the mirror are typically metals and cannot be given additional polishing after aluminizing. A disadvantage of this method is that the reflecting surface eventually corrodes, and destroys the mirror shape.

- Elastic deformation methods:
  In these methods the elasticity of the material is used to achieve a desired deflection under prescribed forces, either by the stressed lap method or the stressed mirror method. Obviously, these techniques are limited by the

level of stress in the mirror. A best-fitting sphere can be used to reduce the induced stresses [33].

It is very difficult to polish non spherical convex mirrors with high accuracy. Concave mirrors are much easier to manufacture.

Generally, a concave surface is also easier to measure than a convex one in optical tests. It is possible to obtain an identical non spherical convex mirror of accurate shape by the replication method. A replicated mirror is composed of a substrate overlaid with a resin layer and moulded on the polished surface of a master. The resin surface is coated with a reflecting layer. Since different materials used in the substrate and resin have different coefficients of thermal expansion, temperature changes will affect the figuring precision. Shrinkage of the resin can also affect the mirror's precision. This method is not suitable for aspheric mirrors with extreme asphericity or fast focal ratio. The secondary mirror of the proposed SDT is a good candidate to produce by the replication method.

The elastic deformation methods are useful for astronomical mirrors in most cases. Many aspherical mirrors have been developed by these methods [6][10][26][28] [29][35].

1.3 Review of Literature

Plates have been studied extensively since the last half of the nineteenth century. Detailed accounts of plate theory can be found in texts by Timoshenko [31][32]. The first aspherical surface made by the elastic deformation of glass was by Schmidt [30] who developed an axisymmetric correcting lens for the Schmidt telescope in 1930, using a rigid full size lap to grind and polish a stressed glass plate. The execution for the Schmidt plate where provided by Couder [7] in 1940.

In 1964 and 1972, Clark [5] and Cox [8] produced some corrector plates by means of this method. Everhart [9] followed Schmidt's classic method and gave a general description in 1966. The desired figure is achieved while the plate is deformed with partial vacuum on the one side. Elastic deformation methods have also been discussed by Lemaitre [13]–[16] to obtain a large variety of aspheric surfaces. The technique for fabricating off-axis paraboloid surfaces was also described by Lemaitre. Variations in plate thickness are deliberately introduced to determine a set of required deflections governed by external loads. Leonard and Alvarez [17] have described a related idea of bending a given surface into another surface by means of a warping harness used to adjust the astigmatism. Lubliner and Nelson [19] developed and demonstrated the elastic deformation technique for production of an off-axis paraboloid segment. The Love's[18] elastic theory was used to obtain the high accuracy of the plate deformation under the necessary forces.

It is known that very good quality spherical mirrors can be produced by rubbing two spheres of equal size together. The spherical polished surfaces currently reach the needed quarter wave accuracy of the Rayleigh rule, or of other absolute accuracy criteria such as that by Marechal [21], which concerns a given intensity distribution at the diffraction pattern.

In principle, the difficulty of polishing aspheres can be reduced to the much simpler one of polishing spheres. A set of forces is applied at several points around the edge of a plate along with an uniform pressure on the back of the plate. The required deflection may be developed under such forces. After a sphere has been ground and polished into the deformed mirror blank, this mirror will deform elastically into the desired nonaxisymmetric paraboloid surface as long as the material used behaves elastically. In principle, the aspheric surface so produced has the same accuracy as the spherical fabrication. Since the basis of the method is to deform the mirror blank elastically, the technique is limited to those cases in which the internal stresses remain below the the material elastic

limit. Thus an extremely aspheric mirror would not be a good candidate for this method.

The recent work on the stressed lap method by Martin et al.[22], applies the elastic deformation method to the fabrication of a paraboloid mirror with a focal ratio of $f/1$. The solutions are expressed in an analytical form for paraboloid mirrors. It is assumed that the lap to be deformed has ideal elastic properties and the deflection is kept small by limiting the diameter of the lap. The stressed lap method can produce an aspheric mirror with high asphericity and a fast focal ratio. The figuring accuracy is achieved by changing lap shape to match the required surface and the lap deflection error is limited to less than $10\mu m$ [23]. The iterative approach can then be used to improve the figuring accuracy of the mirror.

A general function of deflection for an aspheric mirror developed in this thesis is presented as a power-series in chapter 2. In chapter 3 the basic principle of the elastic plate theory and the need for finding the load distributions which can produce a desired deflection are discussed. Chapter 4 uses the finite element analysis to evaluate the behaviour of an analytical model for the mirror. The computed results provide some data of interest for the possible form of the plate deflection resulting from combination of the applied forces. Through several finite element models, the adequate number of discrete points along the boundary of the plate where the forces are applied, is determined.

Chapter 5 presents the conclusions and suggestions for future work.

Chapter 2

Deflection Function

2.1 Overview

This chapter begins by adopting a system of global coordinates for describing the shape of a general symmetrically conic mirror used in most optical systems. To identify a nonaxisymmetric conic surface, a local coordinate system needs to be established. The relation between the two coordinate systems can be established by a matrix expression. A deflection function, suitable for most conic mirrors, is described in the local coordinate system.

2.2 Geometry of Conic Mirrors

It is known that the shape of an optical mirror, using the cylindrical coordinate system may be expressed by the power series in the cylindrical coordinate system [1]:

$$\omega(r,\theta) = \sum A_{mn} r^m \cos n\theta \tag{2.1}$$

where m and n are positive integers, $m \geq n$ and $m - n$ is even, with the restriction that for $m > 6$, the nonvanishing coefficients A_{mn} are those between $m = n$ and $m = n + 2$. With these restrictions, all the commonly used optical

mirrors may be described by Eq.(2.1). By means of elastic plate theory and the proper application of the load distributions around the edge of a plate, the plate may be deformed into any surface described by Eq.(2.1). The relation between the parameters of the conic surface and the coefficients in Eq.(2.1) must first be determined.

In a global coordinate system (X, Y, Z), a symmetrically conic mirror of revolution about the Z axis, with a radius of curvature R at vertex, is described by [20]:

$$Z = \frac{S^2}{R + \sqrt{R^2 - (k+1)S^2}} \tag{2.2}$$

where $S=\sqrt{X^2+Y^2}$. k is the conic constant (defined in page 2). The actual shape of the conic mirror depends on the value of k

$k < -1$	hyperboloid
$k = -1$	parabolid
$-1 < k > 0$	ellipsoid rotated about its major axis
$k = 0$	sphere
$k > 0$	ellipsoid rotated about its minor axis

A flat surface can be defined when $R = \infty$.

2.2.1 Development of a General Deflection Function

In order to find an off-axis conic section of the conic mirror, we establish a local coordinate (x, y, z) shown in Fig.(2.1). Let P be a point on the conic mirror having a distance d from the Z-axis. The coordinates of P are $(d, 0, Z_0)$ in the $X - Z$ plane. The x-y plane and the z-axis are tangent and normal to the conic mirror surface at point P, respectively. It is convenient to let $y = Y$.

The local coordinate system (x, y, z) has the origin at P. From Eq.(2.2), we obtain following since $Y = 0$,

$$Z_0 = \frac{d^2}{R + \sqrt{R^2 - (k+1)d^2}} \tag{2.3}$$

The angle ϕ between the X-axis and the x-y plane, which is the slope at $P(d, 0, Z_0)$, is obtained by differentiating Eq.(2.2) with respect to X:

$$\begin{aligned} \tan\phi &= (\frac{dZ}{dX})_d \\ &= \frac{d}{\sqrt{R^2 - (k+1)d^2}} \end{aligned} \tag{2.4}$$

From Fig.(2.1), a transformation between the two coordinate systems may be established by the matrix expression:

$$\begin{bmatrix} X & Y & Z & 1 \end{bmatrix} = \begin{bmatrix} x & y & z & 1 \end{bmatrix} [R_y][T] \tag{2.5}$$

where R_y is a rotation matrix about the y-axis given by

$$[R_y] = \begin{bmatrix} \cos\phi & 0 & \sin\phi & 0 \\ 0 & 1 & 0 & 0 \\ -\sin\phi & 0 & \cos\phi & 0 \\ 0 & 0 & 0 & 1 \end{bmatrix}$$

and $[T]$ is the translation matrix given by

$$[T] = \begin{bmatrix} 1 & 0 & 0 & 0 \\ 0 & 1 & 0 & 0 \\ 0 & 0 & 1 & 0 \\ d & 0 & Z_0 & 1 \end{bmatrix}$$

A nonaxisymmetric conic mirror may be defined in the local coordinate system (x, y, z) by substituting Eqs.(2.4) and (2.5) into Eq.(2.2):

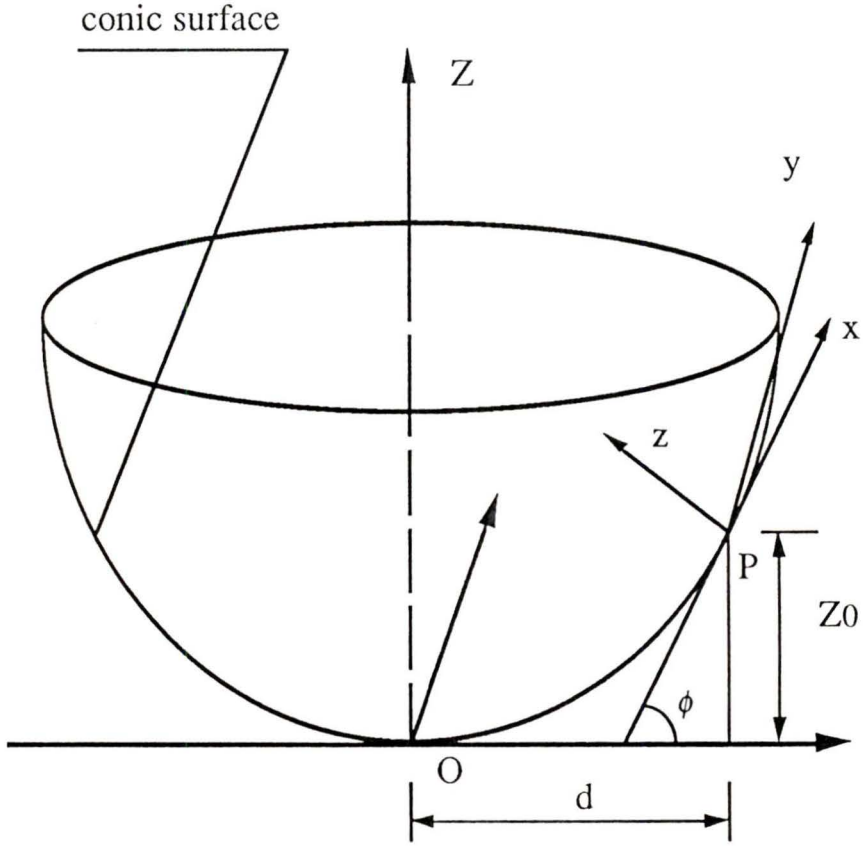

Figure 2.1: Global and local coordinate systems and corresponding geometric parameters

$$z^2[(1+k\cos^2\phi)/R] + 2z[kx\sin\phi\cos\phi/R + [(1+k)Z_0/R - 1]\cos\phi$$
$$-d\sin\phi/R] + (kx^2\sin^2\phi/R + 2x\sin\phi[Z_0(1+k)/R - 1] + x^2/R$$
$$+2dx\cos\phi/R + d^2/R + y^2/R + kZ_0^2/R + Z_0^2/R - 2Z_0) = 0 \qquad (2.6)$$

Eq.(2.6) is a quadratic equation with respect to z. Before solving, this equation may be simplified.

2.2.2 The Simplified Quadratic Equation

A three dimensional curve in a rectangular system (X, Y, Z) may be represented by a position vector $\mathbf{V}$,

$$\mathbf{V}(b) = X(b)\mathbf{e_1} + Y(b)\mathbf{e_2} + Z(b)\mathbf{e_3} \qquad (2.7)$$

for all values of the parameter b in the interval $b_p \leq b \leq b_q$, where $\mathbf{e_1}$, $\mathbf{e_2}$ and $\mathbf{e_3}$ are the unit basis vectors. If we require that $X(b), Y(b), Z(b)$ be single valued functions of the parameter b, then we shall insure that a given value of b defines only one point on the space curve. If the tangent vector exists at point P in Fig.(2.2), the direction of the differential vector $d\mathbf{V}/db$ tends to the direction of the tangent at that point. If we let b become the arc s used as a parameter in Eq.(2.7), namely $\mathbf{V}(s)$, then $\mid \triangle\mathbf{V} \mid$ is equal to $\mid \triangle s \mid$ in the limit. Thus the unit tangent vector $\mathbf{t}$ may be obtained by differentiating the position vector $\mathbf{V}$ with respect to s:

$$\mathbf{t} \equiv \frac{d\mathbf{V}}{ds} = \frac{dX}{ds}\mathbf{e_1} + \frac{dY}{ds}\mathbf{e_2} + \frac{dZ}{ds}\mathbf{e_3} \qquad (2.8)$$

since

$$(ds)^2 = (dX)^2 + (dY)^2 + (dZ)^2 \tag{2.9}$$

the scalar product

$$\mathbf{t} \cdot \mathbf{t} = 1 \tag{2.10}$$

If we differentiate Eq.(2.10) with respect to s, then the scalar product

$$\mathbf{t} \cdot \frac{d\mathbf{t}}{ds} = 0 \tag{2.11}$$

This result indicates that the vector $\mathbf{n} \equiv d\mathbf{t}/ds$ is perpendicular to $\mathbf{t}$. So, $\mathbf{n}$ must be the normal vector at point P.

By means of the above results we can determine both the tangent and normal vectors at P for the conic surface shown in Fig.(2.1). Since we only consider the curve in the $X - Z$ plane, $Y = 0$, the unit tangent vector $\mathbf{t}$ at point P is given by

$$\begin{aligned} \mathbf{t} &= \frac{dX}{ds}\mathbf{e_1} + \frac{dZ}{ds}\mathbf{e_3} \\ &= \frac{dX}{ds}\mathbf{e_1} + \frac{dZ}{dX}\frac{dX}{ds}\mathbf{e_3} \\ &= \frac{dX}{ds}(\mathbf{e_1} + \frac{dZ}{dX}\mathbf{e_3}) \end{aligned} \tag{2.12}$$

From Eq.(2.9),

$$\begin{aligned} (ds)^2 &= (dX)^2 + (dZ)^2 \\ &= (dX)^2 + (\frac{dZ}{dX}dX)^2 \\ &= (dX)^2((\frac{dZ}{dX})^2 + 1) \end{aligned} \tag{2.13}$$

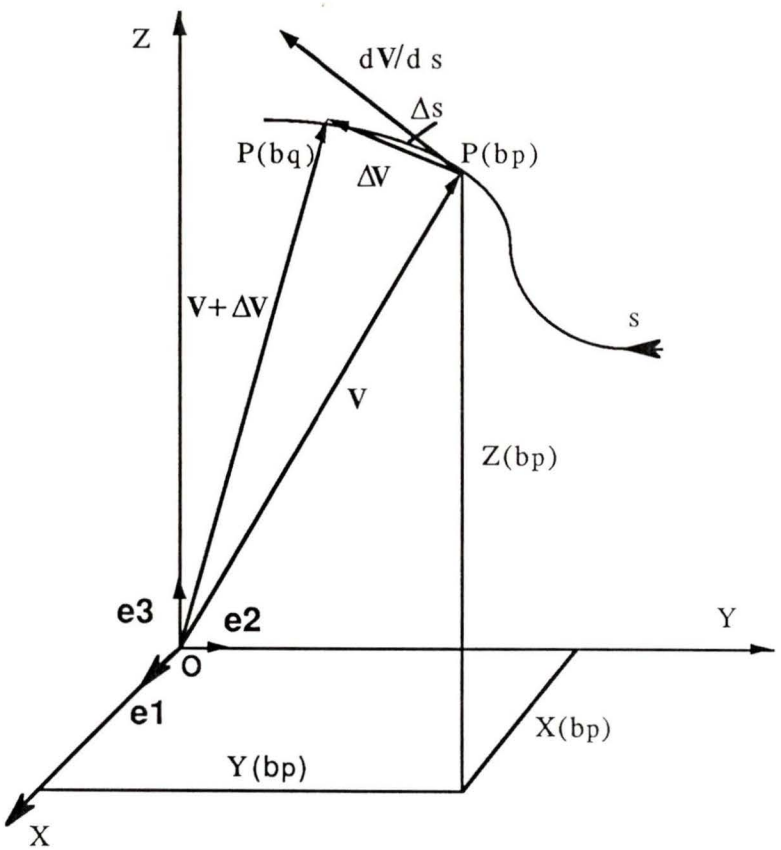

Figure 2.2: Position vector and tangent vector at point P.

Thus

$$\mathbf{t} = \frac{\mathbf{e_1} + dZ/dX\,\mathbf{e_3}}{\sqrt{(dZ/dX)^2 + 1}}$$

where dZ/dX is given by Eq.(2.4). The tangent unit vector may then be expressed as

$$\mathbf{t} = \frac{\mathbf{e_1} + \hbar\mathbf{e_3}}{\sqrt{\hbar^2 + 1}} \tag{2.14}$$

where $\hbar = dZ/dX\ |_{X=d}$, and d is the off-axis distance from the mirror center.

Likewise the inward unit normal vector $\mathbf{n}$ at point P may be described as

$$\mathbf{n} = \frac{-\hbar\mathbf{e_1} + \mathbf{e_3}}{\sqrt{\hbar^2 + 1}} \tag{2.15}$$

To further simplify Eq.(2.6), some useful relations will be derived from Eq.(2.15). First, the angles between the normal vector at P and the X and Z axes are defined as α and β, shown in Fig.2.3, respectively.

These angles are given by:

$$\cos\alpha = \frac{\mathbf{n}\cdot\mathbf{e_1}}{|\,\mathbf{n}\,||\,\mathbf{e_1}\,|} = \frac{-\hbar}{\sqrt{1+\hbar^2}} \tag{2.16}$$

$$cos\beta = \frac{\mathbf{n}\cdot\mathbf{e_3}}{|\,\mathbf{n}\,||\,\mathbf{e_3}\,|} = \frac{1}{\sqrt{1+\hbar^2}} \tag{2.17}$$

From Fig.(2.3), we have following result:

$$\cos\alpha = -\sin\phi \tag{2.18}$$

$$\cos\beta = \cos\phi \tag{2.19}$$

We obtain following equation from Eq.(2.19):

$$\begin{aligned}\cos\phi &= \frac{1}{\sqrt{1+\hbar^2}} \\ &= \sqrt{1+\frac{d^2}{R^2-(k+1)d^2}} \\ &= \sqrt{\frac{R^2-(k+1)d^2}{R^2-kd^2}} \end{aligned} \tag{2.20}$$

Eq.(2.20) multilied by $R/\sqrt{1+k\sin^2\phi}$ gives:

$$\begin{aligned}\frac{R\cos\phi}{\sqrt{1+k\sin^2\phi}} &= \sqrt{\frac{R^2-(k+1)d^2}{R^2-kd^2}}\frac{R}{\sqrt{1+k\sin^2\phi}} \\ &= \frac{R\sqrt{\frac{R^2-(k+1)d^2}{R^2-kd^2}}}{\sqrt{1+k(1-\cos^2\phi)}} \\ &= \frac{R\sqrt{\frac{R^2-(k+1)d^2}{R^2-kd^2}}}{\sqrt{1+k-k\frac{R^2-(k+1)d^2}{R^2-kd^2}}} \\ &= R\sqrt{\frac{R^2-(k+1)d^2}{R^2-kd^2}}\sqrt{\frac{R^2-kd^2}{R^2}} \\ &= \sqrt{R^2-(k+1)d^2} \\ &= R-(R-\sqrt{R^2-(k+1)d^2}) \\ &= R-(k+1)d^2\frac{R-\sqrt{R^2-(k+1)d^2}}{(k+1)d^2} \\ &= R-(k+1)Z_0 \end{aligned} \tag{2.21}$$

We obtain following equation from Eqs.(2.16) and (2.18):

$$\sin\phi = \frac{d}{\sqrt{R^2 - kd^2}} \tag{2.22}$$

or

$$d = \sin\phi\sqrt{R^2 - kd^2} \tag{2.23}$$

Now squaring both sides of Eq.(2.23), obtaining as follows

$$d^2 = \sin^2\phi(R^2 - kd^2) \tag{2.24}$$

or

$$d^2(1 + k\sin^2\phi) = R^2\sin^2\phi \tag{2.25}$$

or

$$d = \frac{R\sin\phi}{\sqrt{1 + k\sin^2\phi}} \tag{2.26}$$

We have following equation from Eq.(2.26):

$$\sqrt{1 + k\sin^2\phi} = \frac{R\sin\phi}{d} \tag{2.27}$$

We also have following result from Eqs.(2.21) and (2.26):

$$\sqrt{R^2 - (k+1)d^2} = R - (k+1)Z_0 \tag{2.28}$$

Squaring both sides of Eq.(2.28), it becomes

$$(k+1)Z_0^2 - 2RZ_0 + d^2 = 0 \tag{2.29}$$

or

$$kZ_0^2/R + Z_0^2/R - 2Z_0 = -d^2/R \tag{2.30}$$

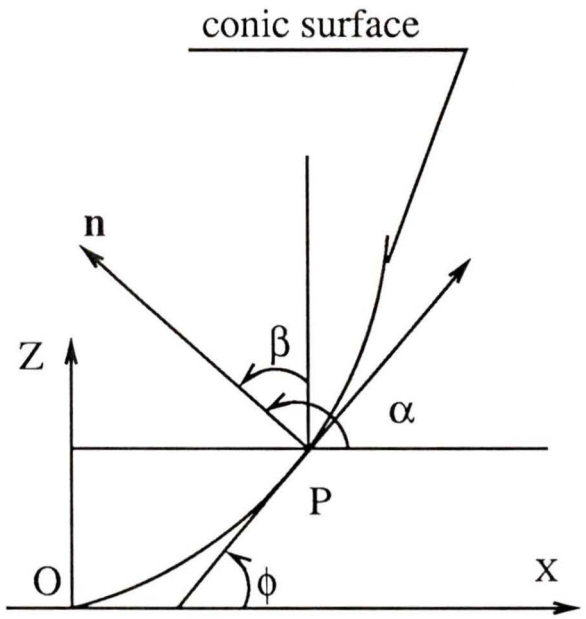

Figure 2.3: Defining the angles about the global coordinate system and the normal vector at point P.

Substituting Eqs.(2.21), (2.26) and (2.30) into Eq.(2.6), the simplified Eq.(2.6) becomes

$$z^2[(1 + k\cos^2\phi)/R] + 2z[kx\sin\phi\cos\phi/R - \frac{1}{\sqrt{1 + k\sin^2\phi}}] + (kx^2\sin^2\phi/R + x^2/R + y^2/R) = 0 \quad (2.31)$$

Eq.(2.31) describes a nonaxisymmetric conic mirror in the local coordinate system when the off-axis distance d is not equal to zero. This equation is still too complicated to be used in the force analysis.

2.3 Solution of Simplified Quadratic Equation

We solve Eq.(2.31) using

$$z = \frac{\eta - \sqrt{\eta^2 - \xi\zeta}}{\xi} \quad (2.32)$$

with

$$\xi = \frac{1 + k\sin^2\phi}{R} \quad (2.33)$$

$$\eta = \frac{1}{\sqrt{1 + k\sin^2\phi}} - \frac{kx\sin\phi\cos\phi}{R} \quad (2.34)$$

$$\zeta = \frac{(1 + k\sin^2\phi)x^2 + y^2}{R} \quad (2.35)$$

We also need to find the relation between the coefficients described by Eq.(2.1) and the conic mirror parameters. So we employ Taylor's series for

a function of two variables. For a function $f(x,y)$ expanded at $(0,0)$, Taylor's series becomes

$$\begin{aligned} f(x,y) &= f(0,0) + x\frac{\partial}{\partial x}f(0,0) + y\frac{\partial}{\partial y}f(0,0) \\ &+ \frac{x^2}{2!}\frac{\partial^2}{\partial x^2}f(0,0) + xy\frac{\partial^2}{\partial x \partial y}f(0,0) + \frac{y^2}{2!}\frac{\partial^2}{\partial y^2}f(0,0) \\ &+ \ldots\ldots + \frac{1}{n!}\sum_{j=0}^{n} x^{n-j}y^j \frac{\partial^n}{\partial x^{n-j}\partial y^j}f(0,0) \\ &+ R_{n+1}(x,y) \end{aligned} \tag{2.36}$$

where the last term is given by

$$R_{n+1}(x,y) = \frac{1}{(n+1)!}(x\frac{\partial}{\partial x} + y\frac{\partial}{\partial y})^{n+1} f(\varrho x, \varrho y) \qquad (0 < \varrho < 1) \tag{2.37}$$

We expand Eq.(2.32) to describe a nonaxisymmetric mirror in the local coordinate system (x,y,z), as a power series. We denote it by z_{non}. We employ the MAPLE program, which can give the analytical solution, to solve the two variables Taylor series Eq.(2.36), then obtain the following results

$$\begin{aligned} z_{non} &= \frac{(1+k\sin^2\phi)^{1/2}}{2R}[(1+k\sin^2\phi)x^2 + y^2] \\ &+ \frac{k\sin\phi\cos\phi}{2R^2}(1+k\sin^2\phi)[(1+k\sin^2\phi)x^3 + xy^2] \\ &+ \frac{(1+k\sin^2\phi)^{3/2}}{8R^3}([4k^2\sin^2\phi\cos^2\phi \\ &+ (1+k\sin^2\phi)(1+k\cos^2\phi)]x^2 \\ &+ (1-k\cos^2\phi)y^2)[(1+k\sin^2\phi)k^2 + y^2] + \ldots\ldots \end{aligned} \tag{2.38}$$

Terms up to the fourth order can represent most optical mirrors because the higher order terms are very small and may be neglected.

We use the same procedure for an axisymmetrically conic surface z_{axi} which has a vertex radius l and a conic constant K, the x-y plane tangent to the conic surface at P, and centered at $(0,0,l)$ in the local coordinate system (x,y,z). The constant and linear terms which represent rigid-body displacements are neglected in the expansion. The result is found to be:

$$z_{axi} = \frac{(x^2+y^2)}{2l} + \frac{(x^2+y^2)^2}{8l^3}(K+1) + ... \tag{2.39}$$

It is obvious that $K = 0$, Eq.(2.39) represents a sphere which is tangent to the conic surface at P.

2.4 The General Deflection Function

For a circular plate it is advantageous to work with the cylindrical coordinate system instead of the Cartesian coordinate system. The two systems are related by

$$x = r\cos\theta \qquad y = r\sin\theta \tag{2.40}$$

From trigonometry, we have the following identities

$$\cos^2\theta = \frac{1}{2}(1+\cos 2\theta) \tag{2.41}$$

$$\cos^3\theta = \frac{1}{4}(3cos\theta + \cos 3\theta) \tag{2.42}$$

$$\cos^4\theta = \frac{1}{8}(cos4\theta + 4\cos 2\theta + 3) \tag{2.43}$$

Substituting Eqs.(2.40), (2.41), (2.42) and (2.43) into Eqs.(2.38) and (2.39) give the z_{non} and z_{on} described in cylindrical coordinates.

A deflection function ω which describes a general conic surface can be defined by the difference of Eq.(2.38) and Eq.(2.39). That is

$$\begin{aligned}\omega(\rho,\theta) &= A_{20}\rho^2 + A_{22}\rho^2\cos 2\theta + A_{31}\rho^3\cos\theta + A_{33}\rho^3\cos 3\theta \\ &+ A_{40}\rho^4 + A_{42}\rho^4\cos 2\theta + A_{44}\rho^4\cos 4\theta + ... \end{aligned} \tag{2.44}$$

where $\rho = r/a$ is a dimensionless quantity. The polynomial Eq.(2.44) is the same as Eq.(2.1) with the constraints given in Section 2.2.

2.4.1 Deflection Function of Stressed Lap

The stressed lap method requires the lap surface match the surface of the mirror when the lap grinds and polishes the mirror. It requires the deflection function describing the difference between a nonaxisymmetric and an axisymmetric surfaces. Thus the deflection can be expressed as $\omega = z_{non} - z_{axi}$. Hence, the coefficients A_{mn} in Eq.(2.44) are given by

$$\begin{aligned}
A_{20} &= -\frac{a^2}{2R}[\frac{R}{l} - \frac{1}{2}(2 + k\sin^2\phi)\sqrt{1 + k\sin^2\phi}] \quad (focus) \\
A_{22} &= \frac{a^2}{4R}k\sin^2\phi\sqrt{1 + k\sin^2\phi} \quad (coma) \\
A_{31} &= \frac{a^3}{8R^2}k\sin\phi\cos\phi(1 + k\sin^2\phi)(4 + 3k\sin^2\phi) \quad (astigmatic) \\
A_{33} &= \frac{a^3}{8R^2}k^2\cos\phi\sin^3\phi(1 + k\sin^2\phi) \\
A_{40} &= -\frac{a^4}{8R^3}((\frac{R}{l})^3(K+1) - \frac{(1 + k\sin^2\phi)^{3/2}}{8}(4k^2\sin^2\phi\cos^2\phi \\
&+ (1 + k\sin^2\phi)(1 + k\cos^2\phi))[(4 + 3k\sin^2\phi) + (1 + k\cos^2\phi)(4 + k\sin^2\phi)]) \\
A_{42} &= \frac{a^4}{16R^3}(1 + k\sin^2\phi)^{3/2}((4k^2\sin^2\phi\cos^2\phi + (1 + k\sin^2\phi)(1 \\
&+ k\cos^2\phi))(1 + k\sin^2\phi) - (1 + k\cos^2\phi))
\end{aligned} \tag{2.45}$$

$$A_{44} = -\frac{a^4 k \sin^2\phi}{64R^3}(1+k\sin^2\phi)^{3/2}((1+k\cos^2\phi) - (4k^2\sin^2\phi\cos^2\phi$$
$$+ (1+k\sin^2\phi)(1+k\cos^2\phi)))$$
$$.....$$

where a is the radius of the plate. We note that the conic constants in both Eqs.(2.38) and (2.39) are the same value (that is, $K = k$).

2.4.2 Deflection Function of Stressed Mirror

The stressed mirror method requires the deflection function describing the difference between a sphere which is defined in Eq.(2.39) with $K = 0$, denoted by z_{sph} and an asphere z_{non}. Thus the deflection function is expressed as $\omega = z_{sph} - z_{non}$. Hence, the coefficients A_{mn} in Eq.(2.44) are given by

$$A_{20} = \frac{a^2}{2R}[\frac{R}{l} - \frac{1}{2}(2+k\sin^2\phi)\sqrt{1+k\sin^2\phi}] \quad (focus)$$

$$A_{22} = -\frac{a^2}{4R}k\sin^2\phi\sqrt{1+k\sin^2\phi} \quad (coma)$$

$$A_{31} = -\frac{a^3}{8R^2}k\sin\phi\cos\phi(1+k\sin^2\phi)(4+3k\sin^2\phi) \quad (astigmatic)$$

$$A_{33} = -\frac{a^3}{8R^2}k^2\cos\phi\sin^3\phi(1+k\sin^2\phi)$$

$$A_{40} = \frac{a^4}{8R^3}((\frac{R}{l})^3(K+1) - \frac{(1+k\sin^2\phi)^{3/2}}{8}(4k^2\sin^2\phi\cos^2\phi \qquad (2.46)$$
$$+ (1+k\sin^2\phi)(1+k\cos^2\phi))[(4+3k\sin^2\phi) + (1+k\cos^2\phi)(4+k\sin^2\phi)])$$

$$A_{42} = -\frac{a^4}{16R^3}(1+k\sin^2\phi)^{3/2}((4k^2\sin^2\phi\cos^2\phi + (1+k\sin^2\phi)(1$$
$$+ k\cos^2\phi))(1+k\sin^2\phi) - (1+k\cos^2\phi))$$

$$A_{44} = \frac{a^4 k \sin^2\phi}{64R^3}(1+k\sin^2\phi)^{3/2}((1+k\cos^2\phi) - (4k^2\sin^2\phi\cos^2\phi$$
$$+ (1+k\sin^2\phi)(1+k\cos^2\phi)))$$

.....

In order to estimate the deflection function derived, we compare Eq.(2.44) with Nelson's work[24] by using the same data given by Nelson (for details, see Appendix A). The results show that Eq.(2.44) is reliable to be used.

Chapter 3

Basic Principle of Elastic Deformation

3.1 Overview

In the following sections the distributions to generate a deflection described by Eq.(2.44) in a plate will be determined. Generally, this is a straightforward problem in elastic plate theory[31] when the plate is considered as a linearly elastic and isotropical material with constant thickness.

3.2 Differential Equation for Plate Deformation

All structures are three-dimensional, and the exact analysis of stress in them presents formidable difficulties. However, such precision is seldom needed, nor indeed justified, for the magnitude and distribution of the applied loading, and the strength and stiffness of the structural material, are not known accurately. For this reason it is adequate to analyze certain structures as if they are one or two-dimensional. Thus the engineer's theory of plates is two-dimensional. Thin plates characterized by the fact that the thickness is small compared with other linear dimensions, may be analyzed in a two-dimensional manner. The simplest

and most widely used plate theory is the classical small deflection theory [31] which is summarized below.

Let us consider a thin plate, in other words, a body with parallel faces and a thickness h which is very small compared to the linear dimension of the faces. We consider a state of stress in an element cut out of the thin plate with an arbitrary small deflection $\omega(x, y)$ as shown in Fig.(3.1). The plane midway between two faces of the element is called middle plane. The thickness of the element denoted by h is considered small in comparison with the other dimensions. The slopes of the middle plane are $\partial\omega/\partial x$ and $\partial\omega/\partial y$. The displacements u_i (i=1, 2) in the x-y plane at a distance z from the middle plane are given by

$$u_i = -z\frac{\partial\omega}{\partial x_i} \tag{3.1}$$

where x and y are denoted by x_1 and x_2 respectively. Therefore the strains in the x-y plane are given by

$$\varepsilon_{ij} = \frac{1}{2}(u_{i,j} + u_{j,i}) \tag{3.2}$$

where $u_{i,j} = \partial u_i/\partial x_j$ (i,j=1, 2). Making use of Hooke's law, the relations between the strains ε_{ij} and stresses τ_{ij} are given in tensor form as follows

$$\varepsilon_{ij} = \frac{1+\nu}{E}\tau_{ij} - \frac{\nu}{E}\delta_{ij}\Theta \tag{3.3}$$

with $\Theta = \tau_{11} + \tau_{22}$, ν is Poisson ratio of the material and E is the Young's modulus.

From the above relations, the expression for the stresses τ_{ij} can be obtained as follows[31]:

$$\tau_{11} = -\frac{Ez}{1-\nu^2}\left(\frac{\partial^2\omega}{\partial x^2} + \nu\frac{\partial^2\omega}{\partial y^2}\right) \tag{3.4}$$

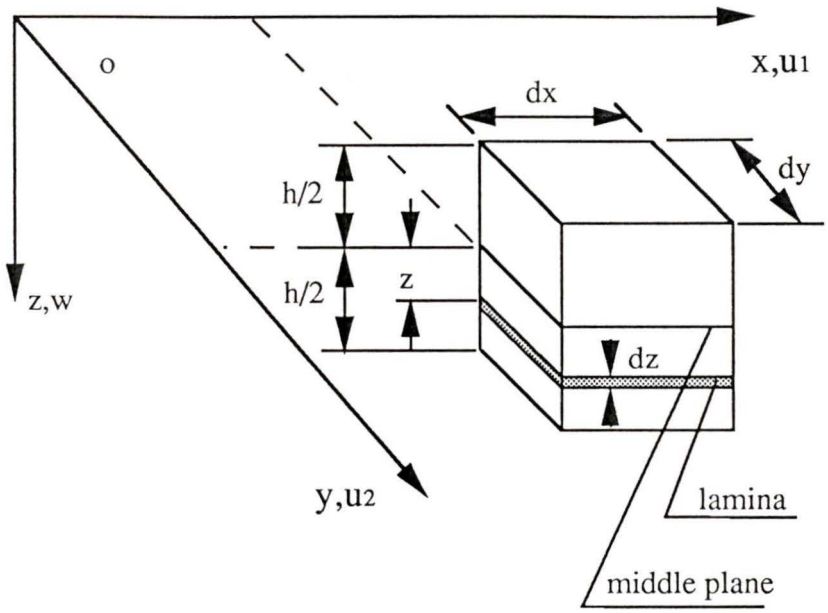

Figure 3.1: An element with an arbitrary small distance z.

$$\tau_{22} = -\frac{Ez}{1-\nu^2}\left(\frac{\partial^2\omega}{\partial y^2} + \nu\frac{\partial^2\omega}{\partial x^2}\right) \tag{3.5}$$

$$\tau_{12} = -\frac{Ez}{1+\nu}\frac{\partial^2\omega}{\partial x \partial y} \tag{3.6}$$

The stresses τ_{ij} vary linearly through the thickness of the plate, and are equivalent to the moments M_{ij} per unit length acting on the lamina given by

$$M_{ij}dx_i = \int_{-h/2}^{h/2} \tau_{ij} z dx_i dz \qquad (i,j = 1,2) \tag{3.7}$$

or

$$M_{ij} = \int_{-h/2}^{h/2} \tau_{ij} z dz \tag{3.8}$$

Substituting the expressions of τ_{ij} into Eq.(3.8), the tensor components in Cartesian coordinates related to the middle plane can be described by

$$M_{ij} = D[(1-\nu)\omega_{,ij} + \nu\delta_{ij}\nabla^2\omega] \tag{3.9}$$

where $\omega_{,ij} = \partial^2\omega/\partial x_i \partial x_j$ and δ_{ij} denotes the Kronecker delta, which is given by

$$\delta_{ij} = \begin{cases} 0 & \text{if} \quad i \neq j \\ 1 & \text{if} \quad i = j \end{cases} \tag{3.10}$$

Suppose that an element bounded by x_i, $x_i + \delta x_i$ is subjected to a distributed normal loading of intensity q, direct along the z-axis direction.

The shearing forces Q_i per unit length are normal to the x_i-axis. Considering the condition of force equilibrium, $\sum F = 0$, it is found [31] that

$$\frac{\partial Q_x}{\partial x}\delta x \delta y + \frac{\partial Q_y}{\partial y}\delta x \delta y + q\delta x \delta y = 0 \tag{3.11}$$

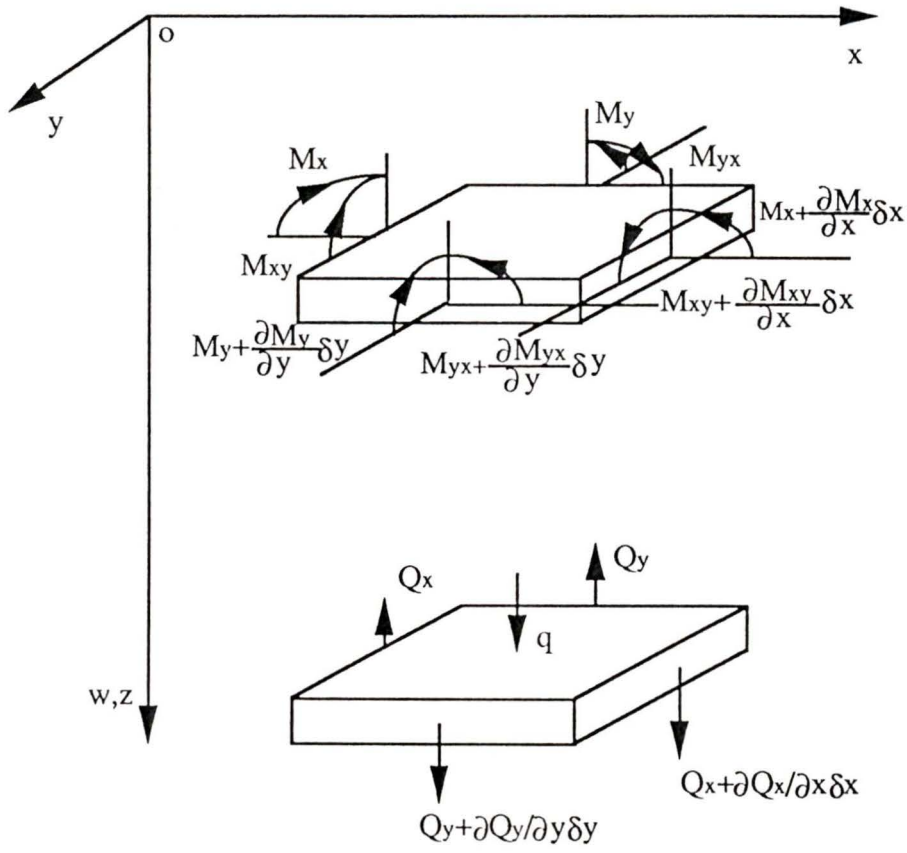

Figure 3.2: Forces acting on a plate element.

or

$$\frac{\partial Q_x}{\partial x} + \frac{\partial Q_y}{\partial y} + q = 0 \tag{3.12}$$

Consider the condition of moment equilibrium, $\sum M = 0$ about the x_i-axis. Taking moments of all the forces acting on the element as shown in Fig.(3.2) with respect to the $x-$axis, the equilibrium equation can be obtained as follows[31]:

$$\frac{\partial M_{xy}}{\partial x}\delta x\delta y - \frac{\partial M_x}{\partial y}\delta x\delta y + Q_y\delta x\delta y = 0 \tag{3.13}$$

or

$$\frac{\partial M_{xy}}{\partial x} - \frac{\partial M_y}{\partial y} + Q_y = 0 \tag{3.14}$$

Likewise, by taking moments with respect to the $y-$axis, we obtain

$$\frac{\partial M_{yx}}{\partial y} + \frac{\partial M_x}{\partial x} - Q_x = 0 \tag{3.15}$$

Obviously, $M_{yx} = -M_{xy}$. Hence,

The shearing forces per unit length acting on the element are given by

$$Q_i = -M_{ij,j} = -D\nabla^2\omega_{,i} \tag{3.16}$$

Since there are no forces in the x and y directions and no moments with respect to the $z-$axis, the above equations completely define the equilibrium of the element shown in Fig.(3.2). Substituting Eq.(3.14) and Eq.(3.15) into Eq.(3.12) to eliminate the shearing forces Q_x and Q_y, we obtain

$$\frac{\partial^2 M_x}{\partial x^2} + 2\frac{\partial^2 M_{xy}}{\partial x \partial y} + \frac{\partial^2 M_y}{\partial y^2} + q = 0 \tag{3.17}$$

To represent this equation in terms of the deflection function ω, Eq.(2.36), we substitute the expressions for M_{ij}, Eq.(3.9) into Eq.(3.17) to obtain the Lagrange's equation [31]

$$D\nabla^2(\nabla^2\omega) = q \tag{3.18}$$

where

$D = Eh^3/12(1-\nu^2)$	The plate stiffness modulus
h	Plate thickness
ν	Poisson ratio of glass
∇^2	Laplacian operator
q	Load applied per unit area

In the polar coordinate system (r, θ), the Laplacian operator is expressed as:

$$\nabla^2 = \frac{\partial^2}{\partial r^2} + \frac{1}{r}\frac{\partial}{\partial r} + \frac{1}{r^2}\frac{\partial^2}{\partial \theta^2} \tag{3.19}$$

If q is a constant, all terms through the forth order described by Eq.(2.44) can be governed by means of the differential Eq.(3.18). For most mirrors, higher than forth order terms are not required because the higher order terms will be very small and be completely negligible in the deflection function.

Since we consider that the plate has an uniform thickness, the values h and D are constant in Eq.(3.18).

3.3 The Forces

It is well known that when a plate is loaded statically, it has an elastic reaction everywhere if the material behaves elastically. The magnitude of elastic reaction is equal to the applied loading and in the opposite direction. In particular, when a plate has a constant thickness h and has a set of forces applied to it, the deflection of the middle plane is governed by Eq.(3.18). The general solution of Eq.(3.18) can be taken in the form of a sum [31]

$$\omega = \omega_1 + \omega_2 \tag{3.20}$$

in which ω_1 is the particular solution and ω_2 is the solution of the homogeneous equation

$$\nabla^4 \omega_2 = 0 \tag{3.21}$$

It is obvious in Eq.(2.44) that $\omega_1 = A_{40} r^4$. If an uniform pressure q is used, the relation between the pressure and the coefficient A_{40} in Eq.(2.44) can be obtained as:

$$q = \frac{64 D A_{40}}{a^4} \tag{3.22}$$

From Eq.(3.9), we may obtain the moments M_r, M_θ and $M_{r\theta}$ per unit length acting on an element. The moments are only related to the deflection given by Eq.(2.44) when plate stiffness modulus D is constant. We write them respectively as follows:

$$M_r = -D[\frac{\partial^2 \omega}{\partial \mathbf{n}^2} + \nu(\frac{\partial \omega}{\partial \mathbf{t}^2})] \tag{3.23}$$

$$M_\theta = -D(\frac{\partial \omega}{\partial \mathbf{t}^2} + \nu \frac{\partial^2 \omega}{\partial \mathbf{n}^2}) \tag{3.24}$$

$$M_{r\theta} = -D(1-\nu)(\frac{\partial^2\omega}{\partial \mathbf{n}^2 \partial \mathbf{t}^2}) \tag{3.25}$$

with **n** and **t** being measured along the normal and the tangent to the side of the element respectively. Eq.(3.9) may be written in polar coordinates by using the following transformations:

$$\frac{\partial^2}{\partial \mathbf{n}^2} = \frac{\partial^2}{\partial r^2} \tag{3.26}$$

$$\frac{\partial^2}{\partial \mathbf{t}^2} = \frac{1}{r}\frac{\partial}{\partial r} + \frac{1}{r^2}\frac{\partial^2}{\partial \theta^2} \tag{3.27}$$

$$\frac{\partial^2}{\partial \mathbf{n}\partial \mathbf{t}} = \frac{1}{r^2}\frac{\partial^2}{\partial r \partial \theta} \tag{3.28}$$

Therefore, moment expressions in polar coordinates are as the following

$$M_r = D[\frac{\partial^2\omega}{\partial r^2} + \nu(\frac{\partial\omega}{r\partial r} + \frac{\partial^2\omega}{r^2\partial\theta^2})] \tag{3.29}$$

$$M_\theta = D(\frac{\partial\omega}{r\partial r} + \frac{\partial^2\omega}{r^2\partial\theta^2} + \nu\frac{\partial^2\omega}{\partial r^2}) \tag{3.30}$$

$$M_{r\theta} = D(1-\nu)(\frac{\partial^2\omega}{r\partial r\partial\theta} - \frac{\partial\omega}{r^2\partial\theta}) \tag{3.31}$$

Likewise, shear forces in polar coordinates are

$$Q_r = -D\frac{\partial}{\partial r}(\nabla^2\omega) \tag{3.32}$$

$$Q_\theta = -D\frac{\partial}{r\partial\theta}(\nabla^2\omega) \tag{3.33}$$

The shearing forces at the boundary (r=a) along the edge are given by [19]

$$V = (Q_r - \frac{\partial M_{r\theta}}{r\partial\theta})_{r=a} \tag{3.34}$$

In the plate boundary the bending moments and shearing forces depend only on θ since the variable r becomes constant at $r = a$. Substituting Eq.(2.44) into the Eqs.(3.29), (3.31) (3.32) and (3.34) we obtain the bending moments and shearing forces expressed as the Fourier series:

$$M(\theta) = M_0 + \sum_{n=1}^{\infty}(M_n \cos n\theta) \tag{3.35}$$

$$V(\theta) = V_0 + \sum_{n=1}^{\infty}(V_n \cos n\theta) \tag{3.36}$$

where the coefficients of both the moment and the shearing force are written in terms of the coefficients of the deflection function as[19]:

$$\begin{aligned} M_0 &= \frac{D}{a^2}[(2+2\nu)A_{20} + 4(3+\nu)A_{40}] \\ M_1 &= \frac{2D}{a^2}(3+\nu)A_{31} \\ V_0 &= -\frac{32D}{a^3}A_{40} \\ V_1 &= -\frac{2D}{a^3}(3+\nu)A_{31} \end{aligned} \tag{3.37}$$

and if $n > 1$,

$$M_n = \frac{D}{a^2}((1-\nu)n(n-1)A_{nn} + (n+1)(n+2-(n-1)\nu)A_{n+2,n} \tag{3.38}$$

$$V_n = \frac{D}{a^3}((1-\nu)n^2(n-1)A_{nn} + n(n+1)(n-4-n\nu)A_{n+2,n}) \tag{3.39}$$

A plate deflection described by Eq.(2.44) can be produced by the above force analysis. By choosing appropriate values of plate thickness h, dimensions of the plate and by controlling the magnitude of the deflection, the classical

plate theory can give an accurate solution. The numerical analysis is illustrated in chapter 4.

3.4 Equilibrium Conditions

The moment and shearing force distributions must be in equilibrium at the plate boundary. The Fig.(3.3) shows the forces applied on a circular plate in equilibrium. After the forces are applied on the plate, the equilibrium condition in the boundary should be checked. The conditions for the equilibrium forces give

$$\int_0^a q2\pi r dr + \int_0^{2\pi} V(\theta) r d\theta = 0 \tag{3.40}$$

or,

$$V_0 = -qa/2 \tag{3.41}$$

Likewise, the moment equilibrium about x and y axes gives

$$\int_0^{2\pi} V(\theta) a^2 \cos\theta d\theta + \int_0^{2\pi} M(\theta) a \cos\theta d\theta = \int_0^{2\pi} \int_0^a qr \cos\theta dr d\theta$$

or,

$$M_1 + aV_1 = 0 \tag{3.42}$$

3.5 Stress Analysis

It is important to check the distribution of stress on the plate when the forces are applied to it. If the maximum stress used is beyond the elastic limit of a material, the formulas derived in this chapter can not be used.

The stress components can be obtained from Eqs.(3.4), (3.5) and (3.6). These stresses are proportional to the distance z of the lamina from the middle plane and also depend upon the magnitudes of the slope of deflection. The stress level increases rapidly when a mirror is extremely thick and severely aspheric. The local maximum of each stress component occurring at $z = \pm h/2$ is given by maximizing the following equation[32]:

$$Maximize(|\tau_1|, |\tau_2|) \tag{3.43}$$

where

$$\begin{bmatrix} \tau_1 \\ \tau_2 \end{bmatrix} = \begin{bmatrix} \frac{\tau_{11}+\tau_{22}}{2} + \sqrt{(\frac{\tau_{11}-\tau_{22}}{2})^2 + \tau_{12}^2} \\ \frac{\tau_{11}+\tau_{22}}{2} - \sqrt{(\frac{\tau_{11}-\tau_{22}}{2})^2 + \tau_{12}^2} \end{bmatrix} \tag{3.44}$$

since the in-plane stress components are assumed to be changed linearly through out the thickness. The stress components can also be described as [19]:

$$\tau_{ij} = -12M_{ij}z/h^3 \tag{3.45}$$

Thus the maximum stress components can be determined by the maximum bending moment components given by[19]

$$\tau_{max} = 6M_{max}/h^2 \tag{3.46}$$

where

$$M_{max} = max \mid \frac{M_t + M_\theta}{2} \pm [(\frac{M_t - M_\theta}{2})^2 + M_{t\theta}^2]^{1/2} \mid \tag{3.47}$$

In the next chapter, we shall consider the details of the numerical analysis in both forces and stresses. We shall also discuss the figuring accuracy simulated by ANSYS program[12], and the method of improving the accuracy.

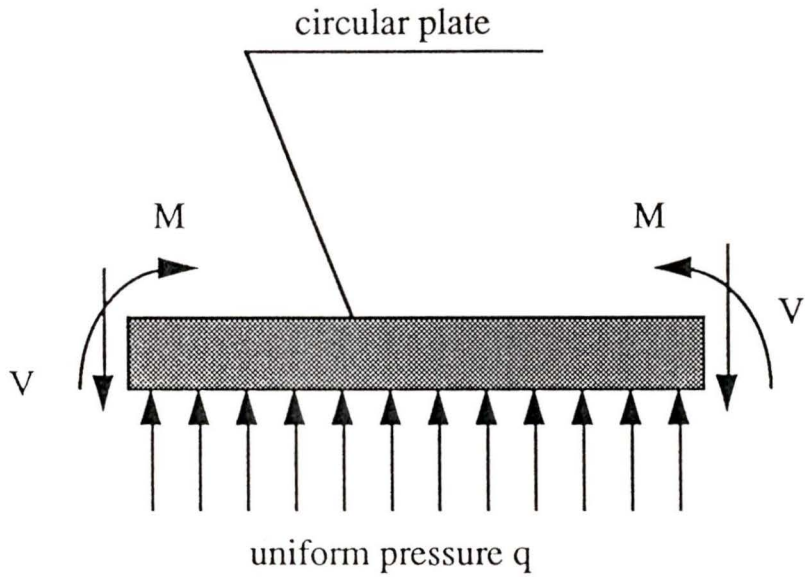

Figure 3.3: Plate with shearing forces, bending moments and uniform pressure in equilibrium.

Chapter 4

Simulation Description and Results

4.1 Overview

In this chapter, the mirror plate is modelled by the finite element method. The geometric parameters of this model are designed by the requirements of the strengths of the material and by figuring accuracy. The elastic thin-plate theory is used to find the required forces, which are applied in the finite element model, to deform the plate into the desired shape. The numerical deflections are then obtained by the ANSYS program[12]. These deflections are then compared with the prescribed deflections given by Eq.(2.44) at corresponding nodes. In this way Eq.(2.44) is matched.

4.2 A Numerical Model for Simulation

The geometric properties of the SDT primary mirror are given in Table 4.1 [27]. The primary mirror has a fast focal ratio and is also very aspheric. These parameters make the primary mirror very difficult to produce by the elastic deformation methods since the necessary stresses required are quite high. However, a theoretical model can be constructed to simulate the mirror. There

are at least three difficulties to consider in such a model. They are the stress level in the material, the size of the deflections and the applicability of the elastic plate theory.

If the required stress is beyond the elastic yield level of the material, the elastic deformation methods cannot be used. When the stress level of the material is below the elastic limit and the geometric parameters of the physical model are properly designed, the elastic plate theory will give very good results. The material responds linearly to the applied forces so long as the internal stress can be maintained in the elastic range.

Table 4.1: Geometric properties of the primary mirror

radius of curvature	conic constant	diameter	focal ratio
2111.0 mm	-1.255	1600.0 mm	f/0.66

One requirement for making stressed polishing mirrors is to find a reasonable arrangement of discrete points where the forces may be applied to accurately induce the desired shapes. Lubliner and Nelson [19] pointed out that the deformed model can be obtained in a plate by a distribution of the forces acting on the edge of the plate. We use the same principle for the simulation test. The proposed finite element model is shown in Figs.(4.1) and (4.2). Twenty-four equally spaced discrete points were chosen along the boundary of the configuration, bearing in mind the required accuracy expected by the finite element analysis. (see Table 4.5, for details). It is made up of ninety-seven nodes and ninety-six elements with six degrees of freedom at each element. On this model various loads, such as pressure, concentrated forces and moments, with either axisymmetric or nonaxisymmetric distribution, may be applied.

4.3 Simulation of Stressed Lap Method

In the stressed lap method a set of forces is applied on the lap to deform its shape elastically so as to match the mirror surface when the lap moves around the mirror surface.

The optical tolerance of the primary mirror for the proposed SDT is not very tight since the focal ratio of the telescope is so short. The figuring shape of the lap is given an allowed error of $10\mu m$ from peak-to-valley[23].

We use the elastic plate theory to design the lap and determine the required forces numerically. First the lap dimension should be determined. Generally, the lap dimension is as small as possible in order to meet the figuring accuracy. A smaller lap will increase the grinding and polishing iteration times. Thus a reasonable size should be selected. We first determine a rigid lap size.

If K is zero in Eq.(2.39), the dimension of the rigid lap can be determined when the value of the maximum deflection given by Eq.(2.44) is less than the allowed error. We have chosen a value of $8\mu m$. The computed results using Eq.(2.44) show that the rigid lap should be less than 30 mm in diameter. Obviously, using such a lap to polish a 1.6 meter-$f/0.66$ mirror would require a long time.

An alternative lap was investigated because if the lap used is actively changing its shape (stressed lap) to match the required shape during grinding and polishing, the dimension of the active lap may be much larger than the rigid one, for the same degree of accuracy. If the lap shape may accommodate changes up to 1 mm and the changes of its shape are controlled to within an accuracy of 1%. Eq.(2.44) gives a lap dimension of 320 mm diameter.

A finite element model is developed based on the correct absolute shape for one position of the lap on the mirror: a distance of 640 mm where it is at the furtherest point from the mirror center. It is the most difficult part to grind and polish on the mirror surface. The maximum deflection measured from the

unstressed lap curve to the stressed one at that point is of 1.039 mm (see Table 4.3, for details).

A 20 mm thick lap was chosen to give it sufficient strength. The diameter-to-thickness ratio is 16:1; the thickness-to-maximum deflection ratio is 20:1. As mentioned previously, these ratios are chosen so that the assumption of thin elastic plate theory may be reasonably satisfied.

The lap consists of a solid aluminum alloy disk. The mechanical properties of the lap are [3][34]:

$$\begin{aligned} \text{Young's modulus } (E) &= 70000\ MPa \\ \text{Poisson's ratio } (\nu) &= 0.33 \end{aligned}$$

Typical allowable stress for such a material is 140 MPa. The unstressed configuration of the finite element model for the lap can be determined by Eq.(2.39). The load distribution can be determined by the formulas derived in chapter 3. The desired forces and moments can be calculated by Eqs.(3.35) and (3.36). Table 4.2 lists the determined values for the forces and moments. By means of finite element analysis, we applied the forces given in Table 4.2 to the model shown in Fig.(4.2), and computed the deflections by using ANSYS program[12]. We estimate the figuring accuracy by comparing the deflections computed by ANSYS with the prescribed deflection calculated by Eq.(2.44) at corresponding nodes. Fig.(4.3) shows that the lap is deformed under the combination of these forces. In order to evaluate the results of the deformed lap, Table 4.3 compares the values of the prescribed and ANSYS deflections at all nodes of the configuration when the lap is located at the farest point from the center of the mirror (see Fig.(4.1), for details of node-number). As expected, the maximum relative error is no more than 1%. The maximum mismatch is $8\mu m$ peak-to-valley and the fitting accuracy is within 3 μm rms. The maximum stress induced in the disk is 69.6 MPa. This is within the allowed stress limit for the aluminum alloy used. An iterative procedure can be used to achieve a

given mirror surface accuracy.

As mentioned by Lubliner and Nelson[19], the shearing forces can be replaced by an equivalent distribution of twisting moments, which are easy to apply in the internal system of the lap.

To check the adequacy of the finite element model a series of runs were made with increasing number of nodes (and therefore degrees of freedom) from the vertex, at the center of the lap, to the lap's edge. Computed results for these runs are shown in Fig.(4.4) where a clear convergence can be seen as the number of the nodes along the lap's radius is increased and quite satisfactory solutions are obtained for four nodes along the radius.

Table 4.2: Pressure, forces and couples applied to lap disk which is located at an off-axis distance $d = 640mm$.

No.of load	Angle $(degree)$	Force (N)	Couple $(\times 10^5\ KN\text{-}mm)$
1	0	2.389	-2.3892
2	15	37.7949	-2.3254
3	30	133.5682	-2.1448
4	45	260.1260	-1.8785
5	60	374.2290	-1.5717
6	75	428.4971	-1.2750
7	90	384.1285	-1.0339
8	105	224.0714	-0.8777
9	120	-37.7274	-0.8132
10	135	-355.3798	-0.8235
11	150	-660.5776	-0.8742
12	165	-880.8712	-0.9257
13	180	-961.1546	-0.9469
14	195	-880.8712	-0.9257
15	210	-660.5776	-0.8742
16	225	-355.3798	-0.8235
17	240	-37.7274	-0.8132
18	255	224.0714	-0.8777
19	270	384.1285	-1.0339
20	285	428.4971	-1.2750
21	300	374.2290	-1.5717
22	315	260.1260	-1.8785
23	330	133.5682	-2.1448
24	345	37.7949	-2.3254
pressure: 47.968 KPa			

Table 4.3: Prescribed and numerical deflections at each node. The prescribed deflections are computed by Eq.(2.44) and the numerical deflections are from ANSYS results. Maximum misfit is 8 μm from peak-to-valley.

node No.	prescribed defl.(mm)	numerical defl.(mm)	node No.	prescribed defl.(mm)	numerical defl.(mm)
1	0	0	29	-0.321	-0.313
2	-0.059	-0.058	30	-0.022	-0.022
3	-0.245	-0.242	31	-0.086	-0.083
4	-0.568	-0.565	32	-0.188	-0.182
5	-1.039	-1.038	33	-0.324	-0.316
6	-0.057	-0.056	34	-0.028	-0.028
7	-0.234	-0.232	35	-0.109	-0.106
8	-0.544	-0.541	36	-0.235	-0.230
9	-0.996	-0.995	37	-0.399	-0.392
10	-0.050	-0.049	38	-0.037	-0.037
11	-0.206	-0.204	39	-0.143	-0.140
12	-0.478	-0.475	40	-0.307	-0.303
13	-0.877	-0.875	41	-0.521	-0.515
14	-0.040	-0.039	42	-0.046	-0.046
15	-0.166	-0.164	43	-0.177	-0.175
16	-0.388	-0.384	44	-0.383	-0.379
17	-0.712	-0.710	45	-0.650	-0.645
18	-0.030	-0.030	46	-0.053	-0.052
19	-0.126	-0.124	47	-0.203	-0.201
20	-0.293	-0.289	48	-0.439	-0.435
21	-0.538	-0.533	49	-0.748	-0.743
22	-0.023	-0.022	50	-0.055	-0.055
23	-0.095	-0.093	51	-0.213	-0.211
24	-0.219	-0.213	52	-0.460	-0.456
25	-0.397	-0.390	53	-0.784	-0.780
26	-0.020	-0.194	54	-0.053	-0.052
27	-0.080	-0.078	55	-0.203	-0.201
28	-0.181	-0.176	56	-0.439	-0.435

Continuing Table 4.3

node No.	prescribed defl.(mm)	numerical defl.(mm)	node No.	prescribed defl.(mm)	numerical defl.(mm)
57	-0.748	-0.743	77	-0.321	-0.313
58	-0.046	-0.046	78	-0.023	-0.022
59	-0.177	-0.175	79	-0.095	-0.092
60	-0.383	-0.379	80	-0.219	-0.213
61	-0.650	-0.645	81	-0.397	-0.390
62	-0.037	-0.037	82	-0.030	-0.030
63	-0.143	-0.140	83	-0.126	-0.124
64	-0.307	-0.303	84	-0.293	-0.289
65	-0.521	-0.515	85	-0.538	-0.532
66	-0.028	-0.028	86	-0.040	-0.039
67	-0.109	-0.106	87	-0.166	-0.164
68	-0.235	-0.230	88	-0.388	-0.384
69	-0.399	-0.392	89	-0.712	-0.707
70	-0.022	-0.021	90	-0.050	-0.049
71	-0.086	-0.083	91	-0.206	-0.204
72	-0.188	-0.182	92	-0.478	-0.475
73	-0.324	-0.316	93	-0.877	-0.875
74	-0.020	-0.019	94	-0.057	-0.056
75	-0.080	-0.078	95	-0.234	-0.232
76	-0.181	-0.176	96	-0.544	-0.541
			97	-0.996	-0.995

4.4 Simulation of Stressed Mirror Method

In the stressed mirror technique the forces are applied on the mirror blank rather than the lap disk. The general idea is to produce a required deflection through application of a set of forces. The blank is then ground by a sphere. After the forces are removed, the spherical surface ground deforms elastically into the desired aspheric surface, for instance a hyperboloid.

The glass CerVit has been chosen as the mirror blank, with the following

mechanical properties[24]:

$$\begin{array}{lcl} \text{Young's modulus } (E) & = & 90000\ MPa \\ \text{Poisson's ratio } (\nu) & = & 0.25 \end{array}$$

The stress level is critical for this approach since the glass blank may break if stresses in it exceed a given level. For this, Nelson et al [24] determined an experimental stress level below 19.6 MPa for safe application.

First, we intended to figure a one-piece mirror using the elastic deformation method. There are two limitations for the stressed mirror technique for one-piece mirrors. One is that a one-piece mirror has an initial curvature before it is deformed; thus the flat plate theory cannot not give a good solution to such cases. The other limitation can be found from deflection Eq.(2.44). The error could not be ignored if $A_{60}\rho^6$ is not included in the deflection function when the focal ratio of the mirror is fast. Lubliner and Nelson[19] pointed out that the stressed mirror technique cannot take account of such high terms (see Eq.(3.18)). Thus we must consider another structure for the primary mirror. One choice is a structure of segmented mirrors.

A segmented mirror consists of a number of mirrors. The segments can be produced by the stressed mirror method one by one. The procedure for finding the forces and moments for a segment is similar to that used in the stressed lap method. We choose a set of thirty-six hexagonal segments to conform to a single hyperboloid surface. This is the maximum number to fit the mirror surface. There are six different surface figures for the mirror segments as shown in Fig.(4.5). The surface figure depends on the off-axis distance d (shown in Fig.(2.1)) from the center of the mirror. The figure type is also numbered in Fig.(4.5).

A segment of the primary mirror, number 3, was chosen for the test: it is the most difficult to produce because of the large deflections required in this position. A best-fitting sphere to the mirror surface was chosen in order to

reduce the stresses in the mirror blank. The parameters of the numerical model are listed bearing in mind the limitations imposed by the stress and stiffness requirements as following:

Radius of segment (a)	=	155.0 mm
Thickness of segment (h)	=	5 mm
Off-axis distance (d)	=	800 mm
Radius of best fit sphere (l)	=	2500.0 mm

The arrangement shown in Fig.(4.6) can be used in the case of stressed mirrors for application of the forces. Obviously it is simpler to apply the forces on the mirror blank than on the lap, because the stressed lap is required to change its shape in different positions and orientations on the mirror as it moves to polish the mirror blank. The best-fitting sphere reduces the maximum value of the deflection from 1.39 mm to 0.492 mm. The diameter-to-thickness and thickness-to-deflection ratios are 31:1 and 60:1 respectively. The forces and moments required are listed in Table 4.4.

Fig.(4.7) shows that the segment is deformed under a set of imposed forces. The maximum value of deflection is 0.492 mm. The circular paths have been constructed at four different radii through all nodes shown in Fig.(4.2). The results are given in Figs.(4.8) and (4.9). The worst mismatch occurs near the segment edge due to the strong astigmatism. The maximum value of mismatch is 3 μm peak-to-valley and the figuring accuracy is 0.5 μm rms. The maximum induced stress on the segment is 14.20 MPa which occurs along the edge of the mirror segment. This is below the stress level proposed by Nelson[24], so breakage is not a problem.

A numerical example of calculating the prescribed displacement and the forces are given in Appendix B.

Table 4.4: Pressure, forces and couples applied to mirror segment which is located at an off-axis distance $d = 800mm$.

No.of discrete	Angle (*degree*)	Force (N)	Couple ($N - mm$)
1	0	2.2261	2235.617
2	15	1.0093	2072.295
3	30	-2.3287	1612.825
4	45	-6.8949	943.419
5	60	-11.3620	190.224
6	75	-14.2382	-506.045
7	90	-14.2480	-1021.659
8	105	-10.7476	-1280.732
9	120	-4.0336	-1276.119
10	135	4.5997	-1071.890
11	150	13.1339	-783.872
12	165	19.3861	-542.460
13	180	21.6796	-449.241
14	195	19.3861	-542.460
15	210	13.1339	-783.872
16	225	4.5997	-1071.890
17	240	-4.0336	-1276.119
18	255	-10.7476	-1280.732
19	270	-14.2480	-1021.659
20	285	-14.2382	-506.045
21	300	-11.3620	190.224
22	315	-6.8949	943.419
23	330	-2.3287	1612.825
24	345	1.0093	2072.295
pressure: 364.910 Pa			

The remaining segments can be fabricated by choosing different values of off-axis distance d (see Fig.(2.1), for details). The maximum stress induced in a mirror segment, when deformed, can be described as a function of offset distance d.

We may determine the maximum stresses when the segments have different off-axis distances. The local maximum stress my be determined when an off-axis distance d is fixed. The local maximum stress can be obtained from either

Eq.(3.41) or Eq.(3.44). An optimization program may be used to search for the values of (x, y) which gives rise to maximum stresses. Two segment sizes of radii, $a_1 = 155\ mm$ and $a_2 = 75\ mm$, with conic constant $k = -1.255$, vertex radius $R = 2111.0\ mm$, and with a thickness $h = 5\ mm$, were chosen to show the relations between the local maximum stresses and off-axis distances of the segments for CerVit glass. Maximum stresses, as a function of off-axis distance d, are plotted in Fig.(4.10). The best-fitting spheres are assumed at each position.

A fair accuracy can be obtained by an iterative polish. If a single polish contains errors of order ϵ_0 and the required deflection is of order ϖ, then after n-th polishing iteration, errors can be approximated as follows [19]:

$$\epsilon_n \sim (\frac{\epsilon_0}{\varpi})^n \varpi \tag{4.1}$$

Usually, the fabricating error is much smaller than the deflection. In the case of the primary SDT mirror, ϵ_0/ϖ is of order 10^{-2} in the first polishing cycle. The stressed mirror technique converges to the required figuring accuracy fast.

A general procedure for the stressed mirror method is illustrated in the flow chart in Fig.(4.11).

4.5 Discussion of the Model

4.5.1 Adequacy of Discrete Points

Most mirrors only require the lower order deflection described in Eq.(2.44). The higher oder deflection terms tend to be very small so that they can be neglected. Thus it is possible to obtain these lower deflection terms by means of applying the forces only along the plate boundary with an uniform pressure on its back. In practice the forces are applied to discrete points along the plate's edge.

It is interesting to consider how many such discrete points should be chosen so that a given accuracy can be ensured. Finite element analysis was performed to determine the adequate number of discrete points. Eight, ten, twelve and twenty-four discrete points along the edge were chosen to apply the necessary forces, respectively. Fig.(4.12) illustrates that the increasing figuring accuracy increases as the number of points are increased. When the discrete points reach twenty four, the numerical profile converges to the analytical one. Accordingly twenty-four discrete edge points were chosen for the simulation of the primary mirror in the previous sections.

Table 4.5 gives the different accuracies associated with different number of discrete points.

Table 4.5: The number of discrete point in lap edge with corresponding accuracy.

Discrete Point Numbers	Maximum Error From Peak-to-valley
8	$33\mu m$
10	$16\mu m$
12	$10\mu m$
24	$8\mu m$

4.5.2 Finding the Best Fit Curvature

The problem of finding the best fitting sphere to a known asphere is one of optimizations. The best-fitting sphere is very useful for the stressed mirror method. This best-fitting sphere to a known aspheric mirror can be determined by minimizing the difference between the sphere and asphere geometry in a least squares manner,

$$\min_{\gamma}[\int_0^{2\pi}\int_0^a \omega^2(r,\theta)rdrd\theta] \tag{4.2}$$

where γ is equal to $1/l$ and ω is described by Eq.(2.44). The sphere is presented by setting $K = 0$ in Eq.(2.39). We substitute Eq.(2.44) with the coefficients given by Eq.(2.46) into Eq.(4.2). The result of integration may be obtained as follows

$$\begin{aligned}\Gamma(\gamma) &= \int_0^{2\pi}\int_0^a \omega^2(r,\theta) r dr d\theta \\ &= \pi a^6[40A_{20}^2 + 60a^2A_{20}A_{40} + 20A_{22}^2 + 30a^2A_{22}A_{42} \\ &+ 15a^2A_{31}^2 + 15a^2A_{33}^2 + 24a^4A_{40}^2 + 12a_4A_{42}^2 + 12a^4A_{44}] \qquad (4.3)\end{aligned}$$

where A_{mn} for $m = 2,3,4$ and $n = 0,1,2,3,4$ are defined by the coefficients of Eq.(2.46) in chapter 2 with $l = 1/\gamma$.

Minimizing Eq.(4.3), we need to differentiate Γ with respect to γ and let the derivatives be equal to zero. Thus

$$20A_{20}A_{20}^{'} + 15a^2A_{20}A_{40}^{'} + 15a^2A_{40}A_{20}^{'} + 12a^4A_{40}A_{40}^{'} = 0 \qquad (4.4)$$

Substituting coefficients A_{20} and A_{40} into the above equation, we obtain the polynomial equation:

$$\begin{aligned}&18a^4\gamma^5 + 120a^2\gamma^3 - 45a^2[(1+\Psi^2)\Psi/R + a^2/20(\Psi/R)^3((1 \\ &+3\Psi^2)(\Psi^2(1+k\cos^2\phi) + 4k^2\sin^2\phi\cos^2\phi) + (1+k\cos^2\phi)(3+\Psi^2))]\gamma^2 \\ &+160\gamma - 80[(1+\Psi^2)\Psi/R + 3a^2/64(\Psi/R)^3((1+3\Psi^2)(\Psi^2(1+k\cos^2\phi) \\ &+4k^2\sin^2\phi\cos^2\phi) + (1+k\cos^2\phi)(3+\Psi^2))] = 0 \qquad (4.5)\end{aligned}$$

where $\Psi = \sqrt{1+k\sin^2\phi}$. It can be expressed as

$$C_5\gamma^5 + C_4\gamma^4 + C_3\gamma^3 + C_2\gamma^2 + C_1\gamma + C_0 = 0 \qquad (4.6)$$

where the polynomial coefficients C_i $(i = 0, 1, ..., 5)$ are given by

$$\begin{aligned} C_0 &= -80[(1+\Psi^2)J + \frac{3a^2}{64}J^3 I] \\ C_1 &= 160 \\ C_2 &= -45a^2[(1+\Psi^2)J + \frac{a^2}{20}J^3 I] \\ C_3 &= 120a^2 \\ C_4 &= 0 \\ C_5 &= 18a^4 \end{aligned} \tag{4.7}$$

and

$$\begin{aligned} I &= (1+3\Psi^2)(\Psi^2\Lambda + 4k^2\sin^2\phi\cos^2\phi) + \Lambda(3+\Psi^2) \\ \Lambda &= 1 + k\cos^2\phi \\ J &= \frac{\Psi}{R} \end{aligned} \tag{4.8}$$

The best-fitting sphere is obtained by solving the polynomial Eq.(4.6). The polynomial equation has at least one real root since its highest term is odd. In Section 4.4, the best-fitting sphere was chosen by the above optimum procedure. At an off-axis distance d equal to 800 mm and a segment diameter of 310 mm, Eq.(4.7) takes on the following values:

$$\begin{aligned} C_0 &= -0.6445 \\ C_1 &= 160 \\ C_2 &= -87.1028 \\ C_3 &= 2.8830 \times 10^4 \\ C_4 &= 0 \\ C_5 &= 1.0390 \times 10^6 \end{aligned}$$

By Abel's principle[2], we cannot find an analytical solution of a polynomial equation of order five or higher. Thus we must use a numerical method such as the Newton-Raphson method[2] to obtain a solution of the polynomial equation. Five roots of Eq.(4.6) are obtained as follows:

$$\begin{aligned} \gamma_{1,2} &= \text{-0.00213} \pm 0.14175\text{j} \\ \gamma_{3,4} &= 0.00012 \pm 0.08757\text{j} \\ \gamma_5 &= 0.0040 \end{aligned}$$

The real root of the polynomial Eq.(4.6) is $\gamma = 0.0040$, hence, $l_{best} = 2500.0\ mm$. Table 4.6 gives the computing results of deflection before and after using the best-fitting sphere for the same segment. By means of the best-fitting sphere, the magnitude of deflections can be reduced rapidly.

Table 4.6: Dependence of deflection on both before and after using the best-fitting spheres.

Stressed Mirror Method (unit: mm)	
l, radius of sphere, segment radius $a = 155.0$	
with off-axis distance 800	
l_{before}=2111.0	$\omega_{max.}$=1.380
l_{best}=2500.0	$\omega_{max.}$=0.492
with off-axis distance 533.0	
l_{before}=2111.0	$\omega_{max.}$=0.733
l_{best}=2272.7	$\omega_{max.}$=0.326

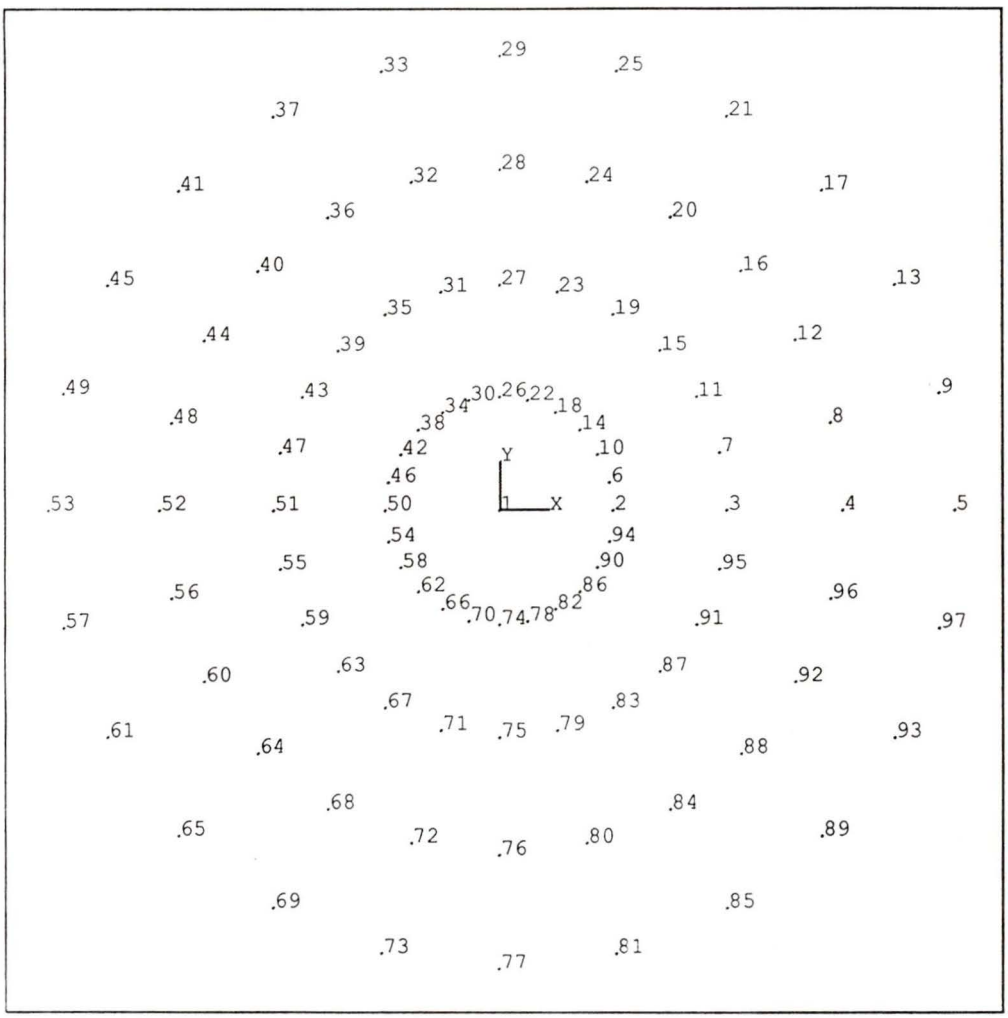

Figure 4.1: Proposed configuration with 97 nodes as an numerical model of finite element analysis.

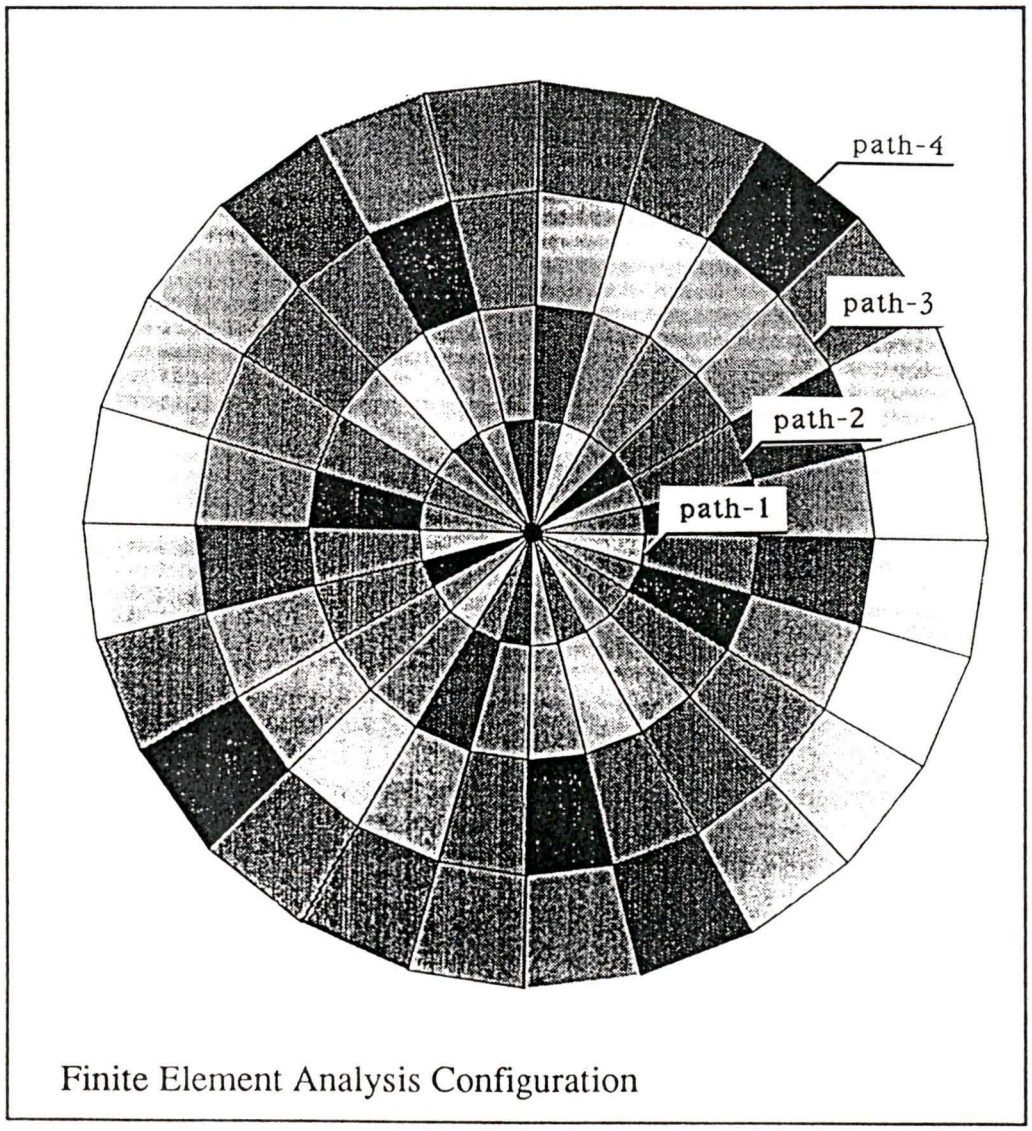

Figure 4.2: Proposed configuration with 96-cell as an numerical model of finite elements and 4 paths modeled.

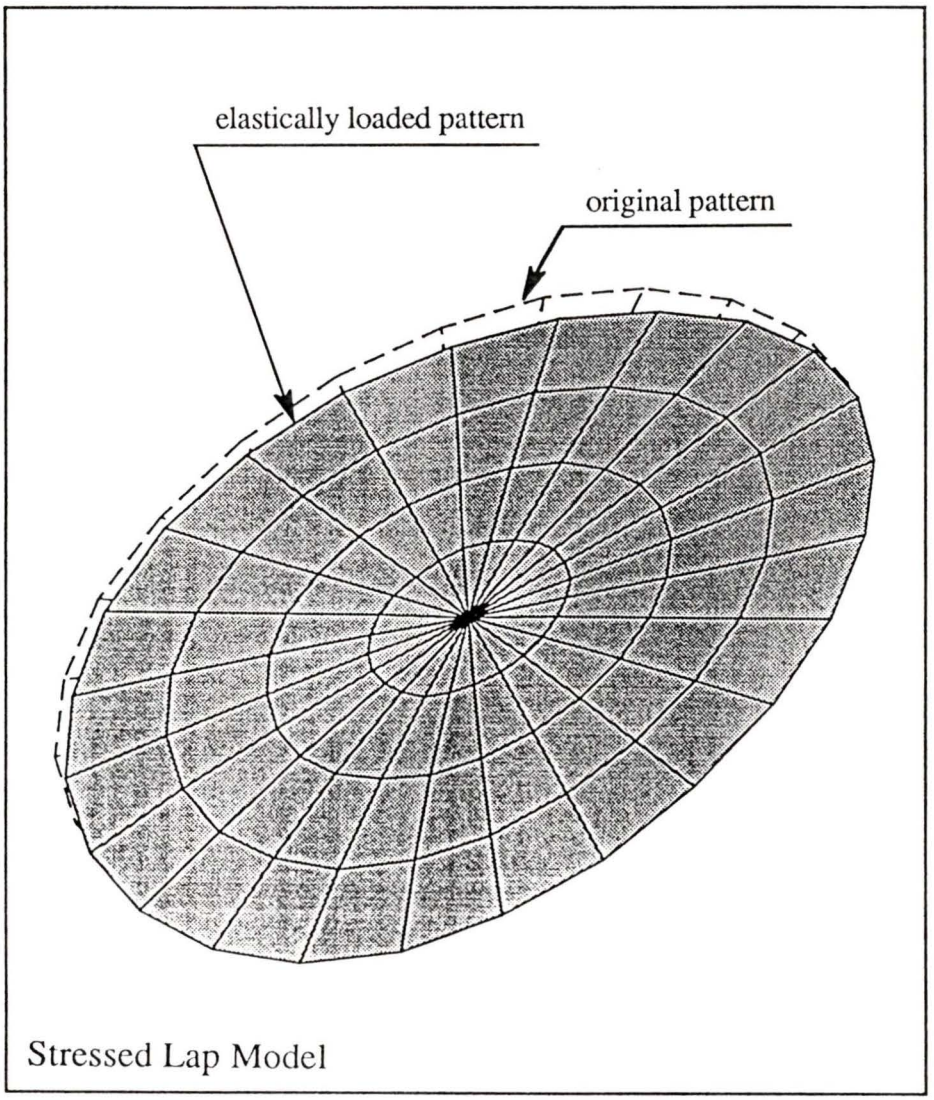

Figure 4.3: The original and elastically loaded patterns of the lap disk.

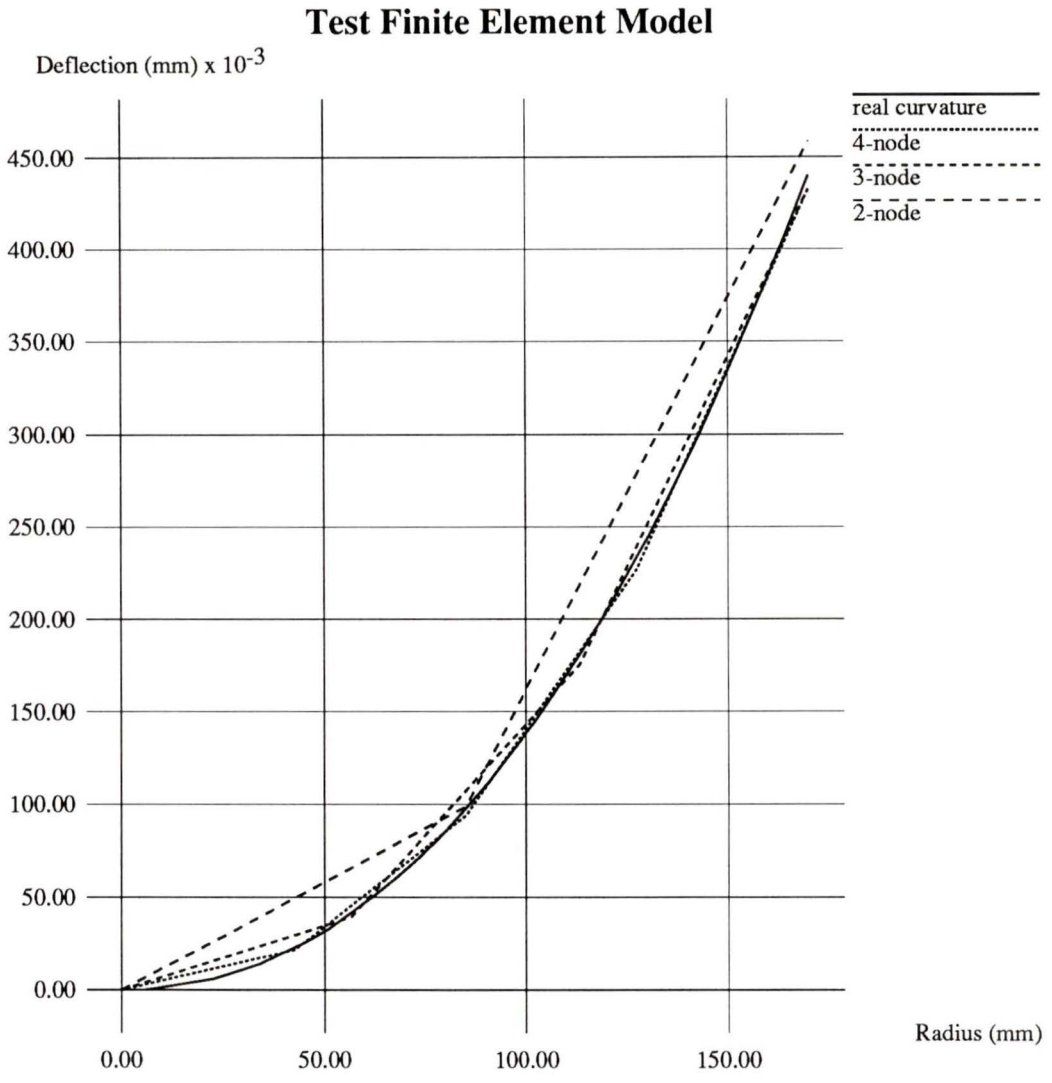

Figure 4.4: Testing configuration model

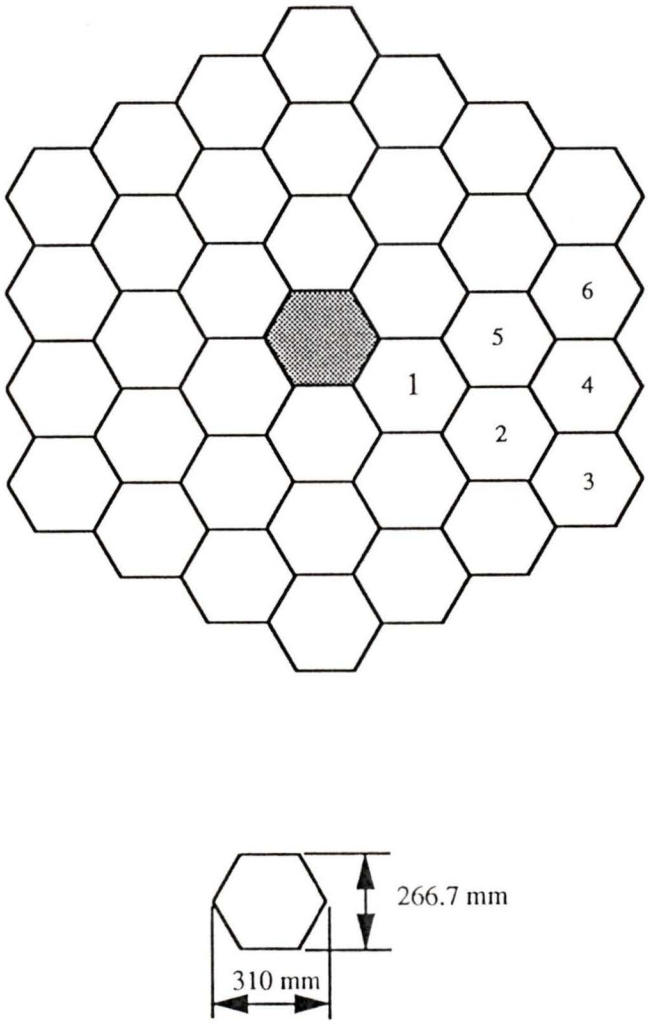

Figure 4.5: Segmentation geometry of the proposed SDT primary mirror with segment surface figure types.

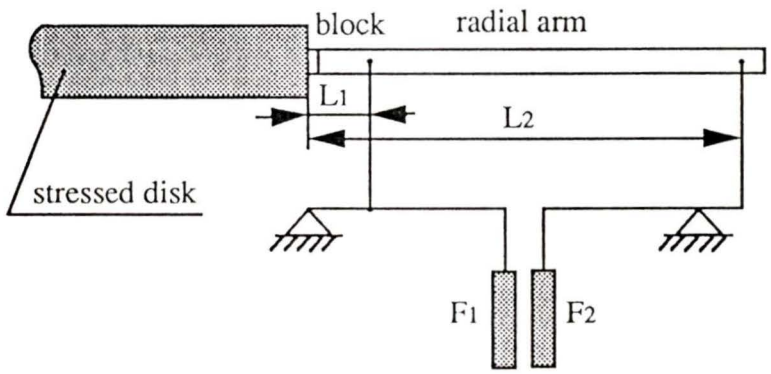

Figure 4.6: Showing the system of applying the forces and moments.

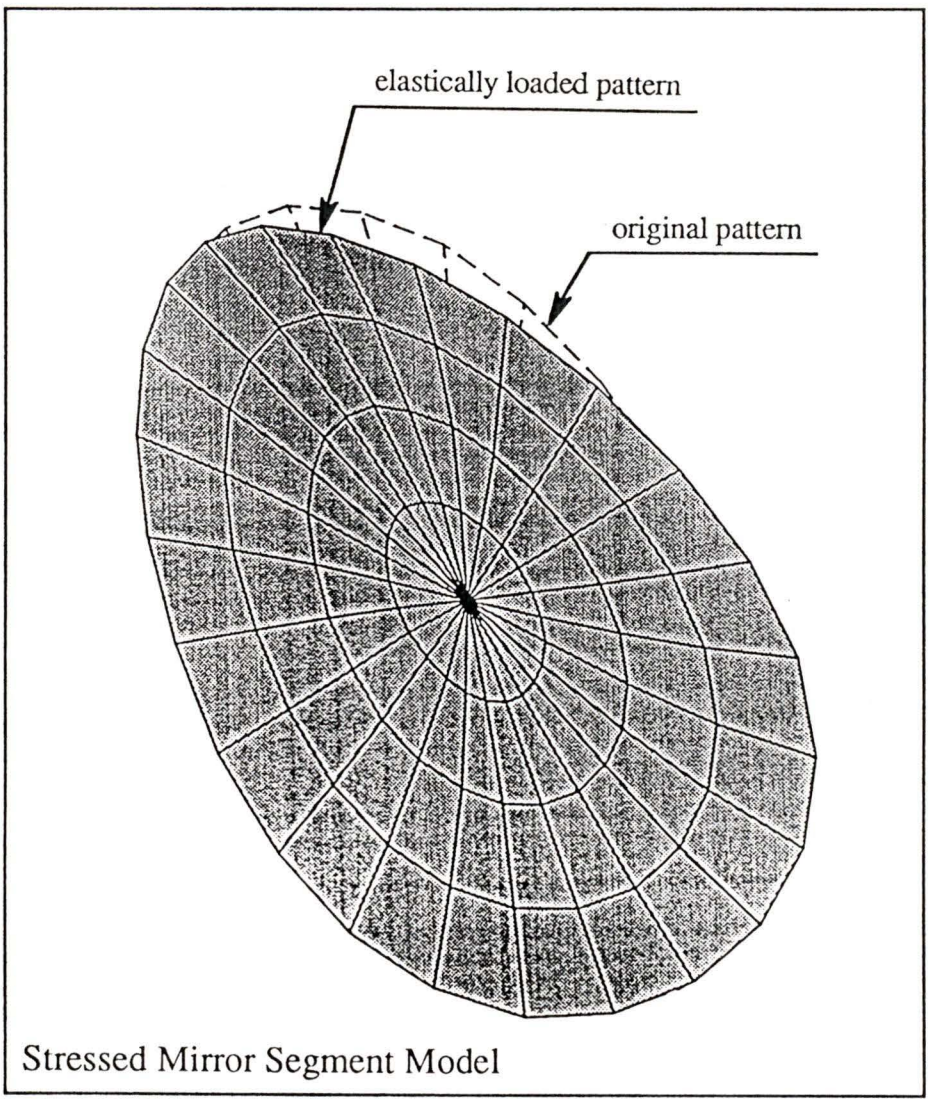

Figure 4.7: The original and elastically loaded patterns of the mirror segment.

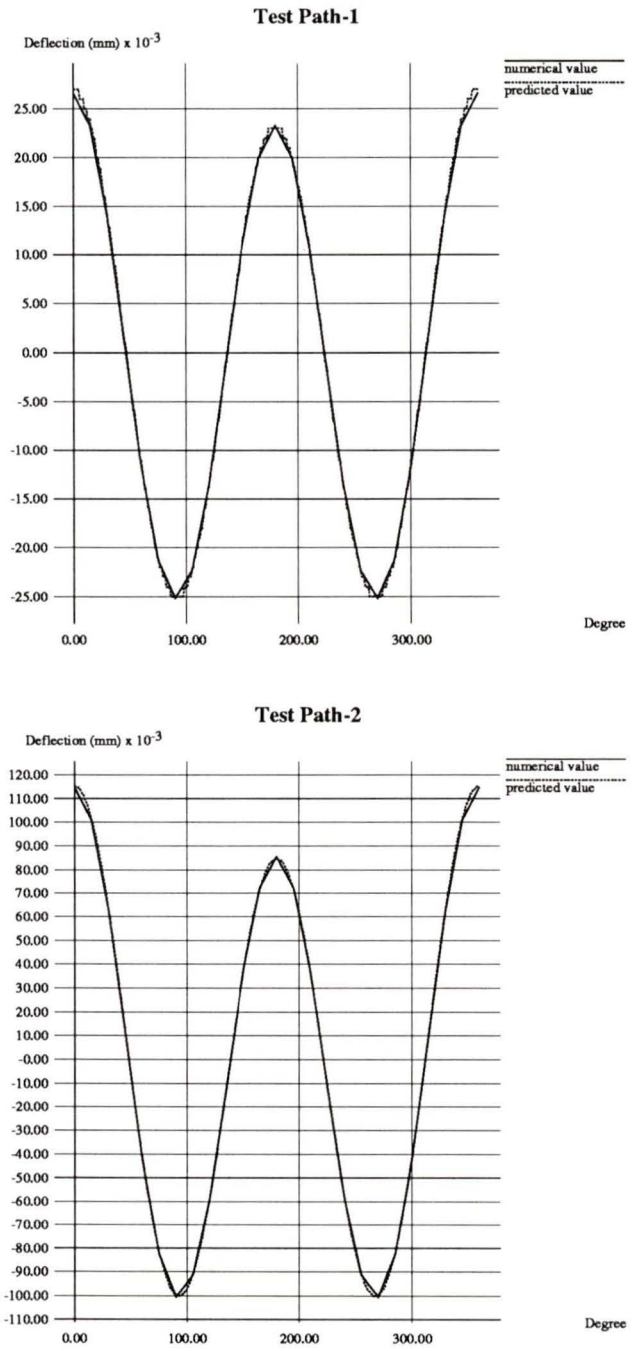

Figure 4.8: Displacement profiles along segment surface. Test Path-1 and Test Path-2 correspond to the first and second path.

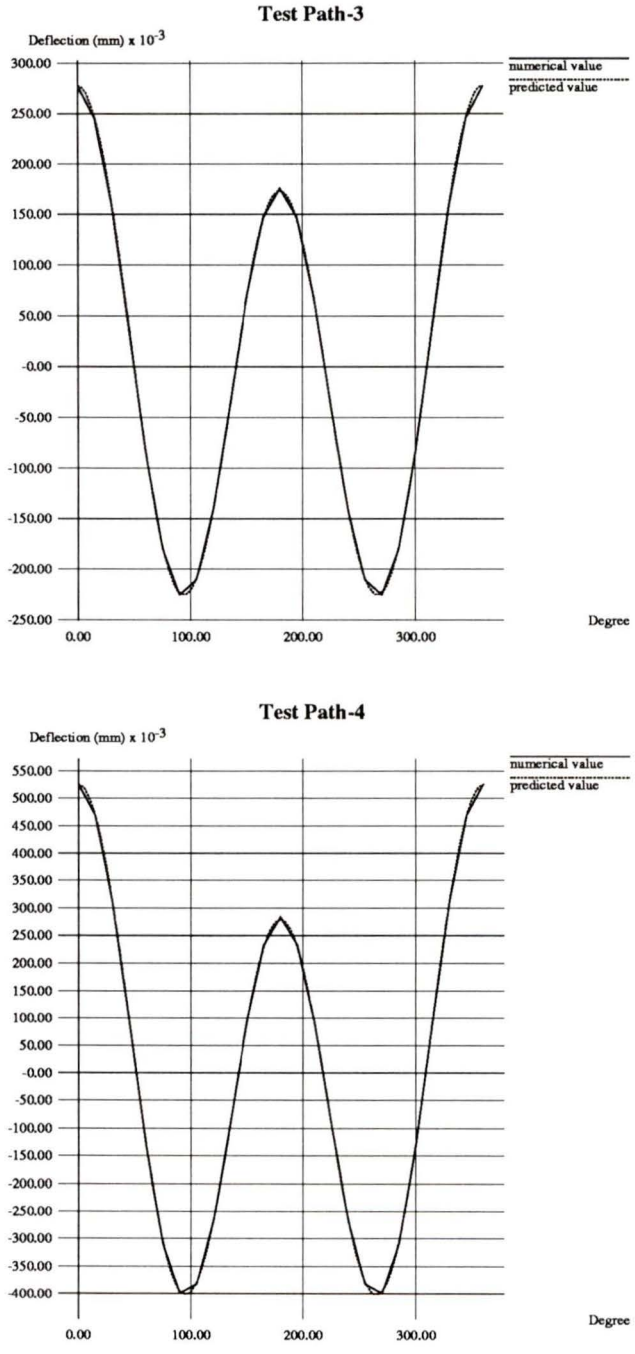

Figure 4.9: Displacement profiles along segment surface. Test Path-3 and Test Path-4 correspond to the third and fourth path.

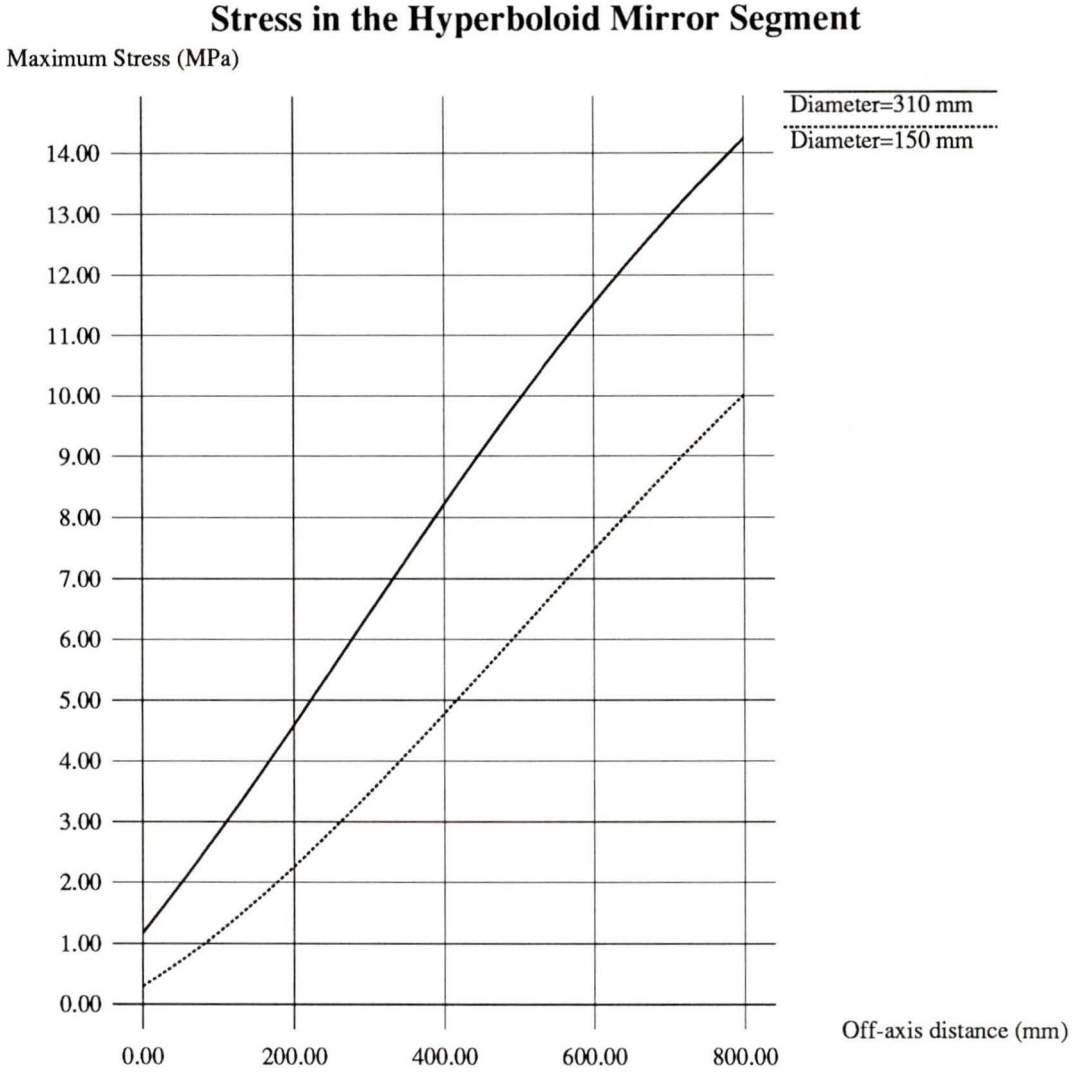

Figure 4.10: Local maximum stress induced in mirror segments during deforming as function of off-axis distance. Best-fitting sphere is used at each position. Hyperboloid segments with different radii: a_1 =155 mm and a_2 =75 mm are plotted.

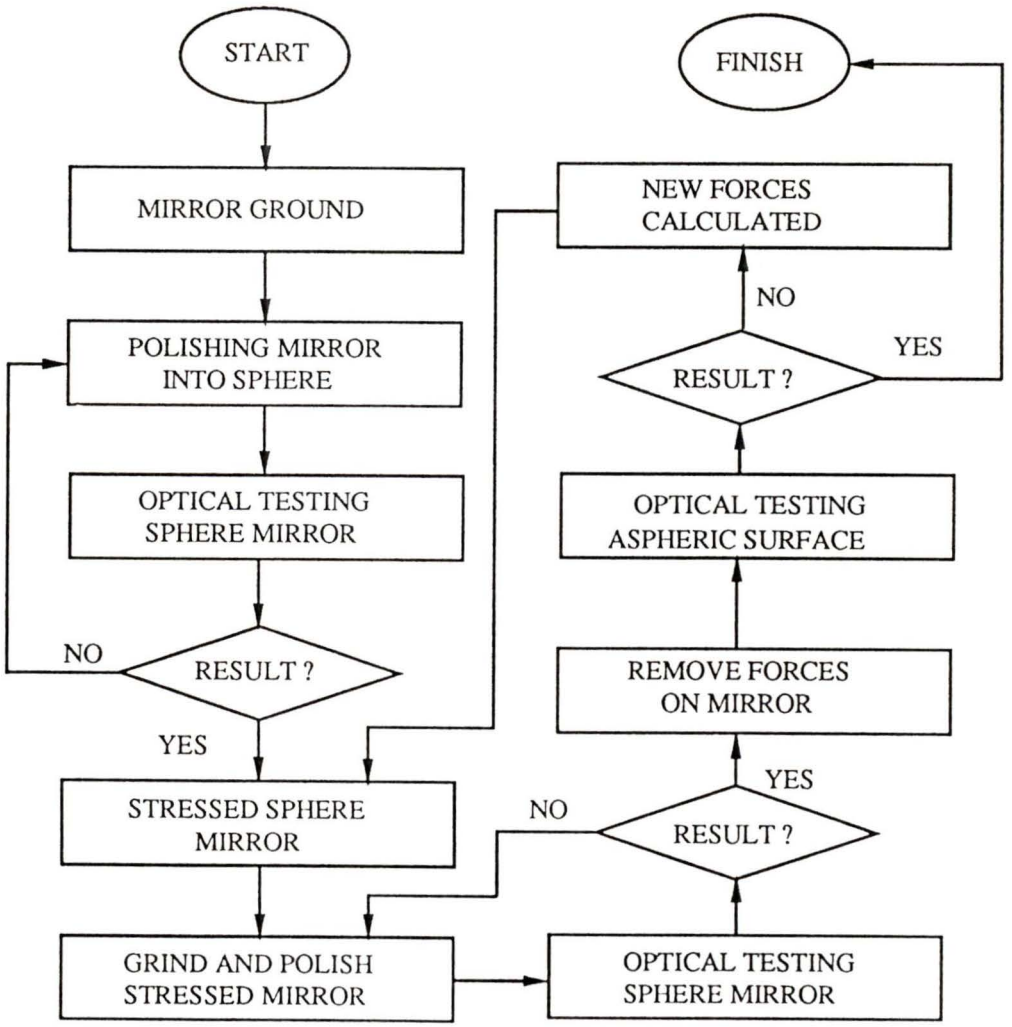

Figure 4.11: General procedure for stressed mirror method.

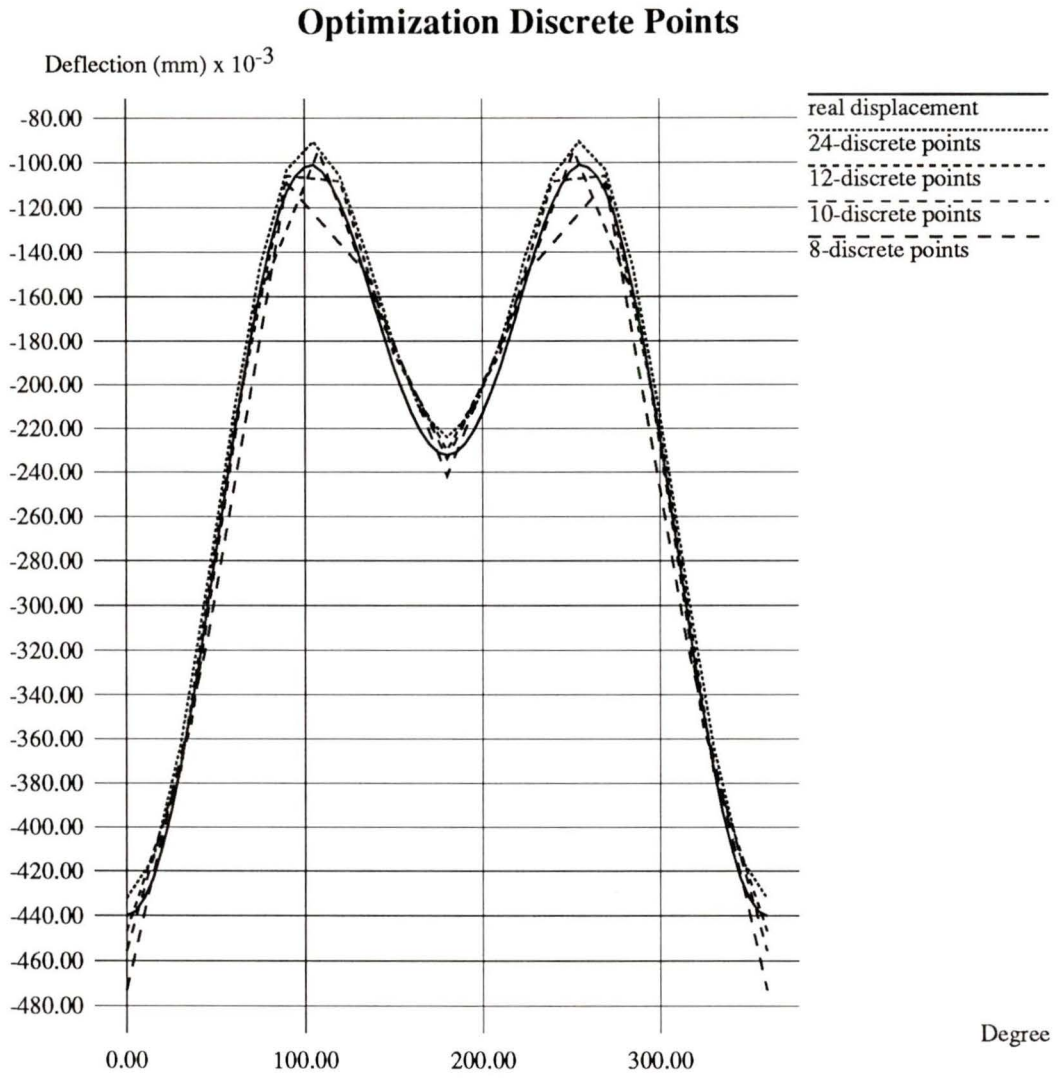

Figure 4.12: Optimizing discrete points in edge of the disk.

Chapter 5

Conclusion and Suggestions for Further Work

5.1 Conclusion

In this thesis, a deflection function which can be used for most aspheric mirrors is derived. This function can describe the deflection between an axisymmetric and a nonaxisymmetric aspheres, or a sphere and a nonaxisymmetric asphere according to the value of the conic constant k used. The feasibility of figuring a mirror is investigated by utilizing the finite element analysis. Both stressed lap and stressed mirror techniques, based on the elastic plate theory, are considered for simulation of the primary mirror of the proposed SDT in a practical manner. The proposed model in figure 4.1 was tested by finite element analysis using different parameters and discrete points in order to analyze the performance characteristics of the model. From the results of the simulations, the capabilities and limitations of the elastic deformation methods to figure the primary mirror can be summarized.

The elastic deformation methods have the primary advantage of generating aspheric mirrors with a desired accuracy in an iterative manner. Thus measurements of error in the fabricated surface can be used to calculate corrective forces, which when reapplied with the original set of forces, will deform the mirror properly for the second grinding and polishing cycle and so on.

It is significant to extend the application of the elastic deformation methods from the paraboloid to the hyperboloid mirrors because the derived general deflection function can be suitable for most optical mirrors (including the paraboloid and spherical mirrors). It offers more information to opticians about how to figure various optical mirrors by means of elastic deformation methods. The procedure of finding a best fitting sphere to a known surface can also be used in a general manner, particularly for the stressed mirror method.

Eq.(4.1) describes that the figuring accuracy may be obtained after the n-th polishing iterations. Generally, the fabrication error ϵ_0 is much smaller than the deflection value. Thus the stressed mirror method converges to the required figuring accuracy rapidly. In principle, this technique allows mirror fabrication of a quality limited only by the quality of the spherical polish. The stress level is important in the sense that if it exceeds some given value, the mirror may break. Since stress is proportional to the deflection required and the thickness of the mirror, the maximum allowed stress level limits the applicability of this technique to mirrors that are not very thick or highly aspheric.

As the primary SDT mirror requires large deflections, due to its fast focal ratio, and severe asphericity, the stressed mirror technique is not suitable to figure a one-piece mirror due to the limitations of the flat plate theory.

The segmented mirror is a good candidate for such a technique since each segment is approximated by a thin flat plate with small deflection. But the segmented mirror would be very complicated and expensive to construct and keep aligned. The figuring accuracy of the segment is limited by the testing procedures since the segment is nonaxisymmetric. For the primary SDT mirror, this model is useful.

In the stressed lap method a small lap is actively flexed to fit the mirror surface. Thus this method may overcome the limitations of the stressed mirror method for producing a one-piece mirror. The stress level with lap can be controlled in a practical manner by choosing appropriate lap dimensions. As

mentioned previously, a large deflection is associated with a smaller lap dimension so the corresponding grinding and polishing will normally be slower. For instance, a paraboloid mirror of diameter 1.8 meter with a focal ratio of f/1 needs a lap diameter about 1/3—the diameter of the mirror [22]; a primary mirror of diameter 1.6 meter with a focal ratio of f/0.66 needs a lap diameter about 1/5—the diameter of the mirror.

It is obvious that the stressed lap system is more complicated than the stressed mirror system because a computer-controlled polishing machine is required in the stressed lap system to actively change the lap shape and match it to the mirror surface. Small polishing zones may remain on the mirror due to the lap being much smaller than the mirror. However, this technique is applicable to the primary SDT mirror.

5.2 Suggestions for Further Work

This model presented here may be applied to the secondary and tertiary mirrors by means of various figuring techniques. As mentioned in chapter 1, the secondary mirror is a good candidate for the replication technique because such a technique is suitable for convex mirrors. The computer-controlled diamond turning technique is able to deal with a very complicated surface no matter what the asphericity is, except for the disadvantage of corrosion in metal blanks.

Bibliography

[1] Born, M. and Wolf, E., *Principles of Optics,* Pergmon, New York, 1970.

[2] Burden, R. L. and Faires, J. D., *Numerical Analysis,* Prindle, Weber & schmidt, Boston, 1986.

[3] Bowes, W. H., Russell, T. and Suter G., *Mechanics of Engineering Materials,* John Wiley and Sons, New York, 1984.

[4] Brueggemann, H. P., *Conic Mirror,* The Focal Press, London, 1968.

[5] Clark, B. A. J., *Journal of Astronomical Society of Victoria,* 6, 76, 1964.

[6] Connes, P. and Micheal, G., "Astronomical Fourier Spectrometer", *Applied Optics,* 14, 9, 2067, 1975.

[7] Couder, A. *Comptes Rendus,* 210, 327, 1940.

[8] Cox, R. E., *Sky and Telescope,* 6, 388, 1972.

[9] Everhart, E., "Making Corrector Plates By Schmidt's Vacuum Method", *Applied Optics,* 5, 5, 713, 1966.

[10] Gabor, G., "Position Sensors And Actuators For Figure Control of A Segmented Mirror Telescope", *Lawrence Berkeley Laboratory, University of California,* 1979.

[11] Golden, L., Gillett, P., Radau, R., Richardon, J., Poczulp, G., "Stressed Mirror Polishing Experiment underway at Kitt Peak National Observatory", *Proceedings of SPIE-The International Society for Optical Engineering,* 332, 357, 1982.

[12] Imgrund, M. C., *ANSYS, Revision 4.3,* Swanson Analysis Systems Inc., 1988.

[13] Lemaitre, G., "New Procedure for Making Schmidt Corrector Plates", *Applied Optics,* 11, 7, 1630, 1972.

[14] Lemaitre, G., "Aspherisation by Elasticity of a 50 *cm* Plate for the Lyon Observatory Schmidt Telescope," *Astronomy and Astrophysics,* 44, 305, 1975.

[15] Lemaitre, G., "Reflective Schmidt Anastigmat Telescopes And Pseudo-Flat Made By Elasticity," *Applied Optics,* 66, 1334, 1976

[16] Lemaitre, G., "Optical Figuring by the Elastic Relaxation Methods", *Current Trends in Optics,* Edited by F. T. Arecchi and F. R. Ausseregg, London, 1981.

[17] Leonard, A. S., "The New Science of Tilted Mirror Optics and Its Application to High Performance Reflecting Telescopes", *Presented at Western Amateur Astronomers and Association of Lunar and Planetary Observers,* San Dieg, 1969.

[18] Love, A. E. H., *Treatise on the Mathematical Theory of Elasticity,* Dover, New York, 1927.

[19] Lubliner, J. and Nelson E., "A Technique for Producing Nonaxisymmetric Mirror", *Applied Optics,* 19, 2341, 1980.

[20] Malacara, D., *Optical Shop Testing,* John Wiley, New York, 1978.

[21] Marechal, G., *Revue d'Optique,* 26, 217, 1947.

[22] Martin H. M., Angel J. R. P. and Cheng, A. Y. S., "Use of An Actively Stressed Lap to polish A 1.8-M F/1 Paraboloid", *ESO Conference on Very Large Telescope and Their Instrumentation,* 353, Garching, March 1988.

[23] Martin, H. M., *Private communication,* Mirror laboratory, University of Arizona, 1990.

[24] Nelson, J. E. and Gabor, G. et al., "Fabrication of An Off-Axis Section of A Paraboloid", *Applied Optics,* 19, 2332, 1980.

[25] Nowlan, F. S., *Analytic geometry,* McGraw-Hill, New York and London, 1934

[26] Paxton, K. B. and Conners, G. H., et al, "Uniform Polishing of Convex Aspheres with an Elastic Lap", *Applied Optics,* 14, 9, 2274, 1975.

[27] Richardson, E. H., et al, "Design of a shuttle-based space debris telescope", *SPIE, Vol.1236, Advanced Technology Optical Telescope IV,* 1990.

[28] Richardson, J. H., "Digest of Workshop on Optical Fabrication and Testing", *Optical Society of America, Washington, D. C.,* April, 1984.

[29] Richardson, J. H., "Stressed Mirror Polishing of a Two-Meter-Diameter Off-Axis Paraboloid", *Journal of the Optical Society of America, Optics and Image Science,* 1984 Annual Meeting.

[30] Schmidt, B., *Mitteilingen der Hamgurger Sternwarte in Bergedorf,* 7, 15, 1932.

[31] Timoshenko, S., *Theory of Elasticity,* McGraw-Hill, New York, 1959.

[32] Timoshenko, S. and Woinowsky-krieger, S., *Theory of Plates and Shells,* McGraw-Hill, New York, 1959

[33] Unti T. W. J., "Best Fit Sphere Approximation to A General Aspheric Surface", *Applied Optics,* 5, 319, 1966

[34] William, H. B., Russell, L. T. and Suter, G. T., *Mechanics of Engineering Materials,* John Wiley and Sons, New York, 1984

[35] Wizinowich, P. and Angel, J. R. P., "A Demonstration of Aspheric Polishing With A Full Size Stressed Lap", *ESO Conference on Very Large Telescope and Their Instrumentation,* 353, Garching, March 1988.

Appendix A

Estimation of Work

In order to estimate the work done, we substitute the data given by Nelson[24] for the parabolic mirror into the deflection function derived in thesis, and set $k = -1$ and $K = 0$ in Eq.(2.44) with the coefficients given by Eq.(2.46). We use the model created in chapter 4, which is of 97-nodes (see Fig.(4.1) and Fig.(4.2), for details). The estimation of work is done by comparing with both deflection functions given by Nelson and Eq.(2.44) to describe the nodal displacement in all nodes.

Table A.1: Parameters of the mirror given by Nelson (unit: cm).

Geometric Parameters of Mirror Segment	
Radius of segment (a)	17.94
Sphere (l)	373.87
Off-axis distance (d)	35.88
Vertex radius of asphere (R)	368.8

The deflections given by Nelson and Eq.(2.44) are calculated. The computing results are listed in Table A.2 as following:

Table A.2: Comparing the numerical results in Eq.(2.44) with the work of Nelson, using the parameters listed in Table A.1 (unit: cm).

	Path-1 nodal displacement		path-2 nodal displacement	
degree	Nelsons'	Thesis'	Nelsons'	Thesis'
0	0.0001	0.0000	0.0003	0.0003
15	0.0000	0.0000	0.0003	0.0002
30	-0.0000	-0.0000	0.0001	0.0000
45	-0.0001	-0.0001	-0.0002	-0.0003
60	-0.0002	-0.0002	-0.0005	-0.0006
75	-0.0002	-0.0002	-0.0008	-0.0008
90	-0.0002	-0.0002	-0.0009	-0.0010
105	-0.0002	-0.0002	-0.0009	-0.0009
120	-0.0002	-0.0002	-0.0008	-0.0008
135	-0.0001	-0.0001	-0.0006	-0.0006
150	-0.0001	-0.0001	-0.0004	-0.0004
165	-0.0000	-0.0000	-0.0002	-0.0002
180	-0.0000	-0.0000	-0.0002	-0.0002
195	-0.0000	-0.0000	-0.0002	-0.0002
210	-0.0001	-0.0001	-0.0004	-0.0004
225	-0.0001	-0.0001	-0.0006	-0.0006
240	-0.0002	-0.0002	-0.0008	-0.0008
255	-0.0002	-0.0002	-0.0009	-0.0009
270	-0.0002	-0.0002	-0.0009	-0.0010
285	-0.0002	-0.0002	-0.0008	-0.0008
300	-0.0002	-0.0002	-0.0005	-0.0006
315	-0.0001	-0.0000	-0.0002	-0.0003
330	-0.0000	-0.0000	0.0001	0.0000
345	0.0000	0.0000	0.0003	0.0002

(continued Table A.2:)

	Path-3 nodal displacement		path-4 nodal displacement	
degree	Nelsons'	Thesis'	Nelsons'	Thesis'
0	0.0011	0.0010	0.0025	0.0024
15	0.0009	0.0009	0.0022	0.0021
30	0.0004	0.0004	0.0013	0.0012
45	-0.0003	-0.0004	-0.0001	-0.0002
60	-0.0010	-0.0011	-0.0015	-0.0016
75	-0.0017	-0.0017	-0.0027	-0.0028
90	-0.0020	-0.0021	-0.0035	-0.0036
105	-0.0021	-0.0022	-0.0038	-0.0039
120	-0.0019	-0.0020	-0.0035	-0.0036
135	-0.0015	-0.0016	-0.0029	-0.0030
150	-0.0011	-0.0011	-0.0022	-0.0023
165	-0.0007	-0.0008	-0.0017	-0.0018
180	-0.0006	-0.0007	-0.0015	-0.0016
195	-0.0007	-0.0008	-0.0017	-0.0018
210	-0.0011	-0.0011	-0.0022	-0.0023
225	-0.0015	-0.0016	-0.0029	-0.0030
240	-0.0019	-0.0020	-0.0035	-0.0036
255	-0.0021	-0.0022	-0.0038	-0.0039
270	-0.0020	-0.0021	-0.0035	-0.0036
285	-0.0017	-0.0017	-0.0027	-0.0028
300	-0.0010	-0.0011	-0.0015	-0.0016
315	-0.0003	-0.0004	-0.0001	-0.0002
330	0.0004	0.0004	0.0013	0.0012
345	0.0009	0.0009	0.0022	0.0021

It is obvious that the maximum mismatch is $1\mu m$ in Table A.2. The results show that Eq.(2.44) is reliable to be used in a practical manner.

Appendix B

A Numerical Example

B.1 Calculation of Displacements

The prescribed nodal displacements listed in Table 4.3 are calculated by Eq.(2.44) with the coefficients given by Eq.(2.45).

The data of the lap geometric dimension and location on the mirror surface are rewritten as following:

Table B.1: The lap location and its geometric parameters.

Lap dimension ($2a$)	310 mm
Lap radius (l)	2500 mm
Conic constant (k)	-1.255
Off-axis distance (d)	800 mm

Substituting the above data into Eq.(2.45), the prescribed nodal displacements are only determined by the positiontion of the node in the lap model described by Figs.(4.1) and (4.2). It is obvious that the nodal displacement given by Eq.(2.44) is the function of angle θ and ρ. For instance, when $\theta = 30°$ and $\rho = 1$, which is determined a edge node number 13 in the lap model (for details, see Fig.(4.1)). We substitute the above data into Eq.(2.45), the coefficients of the displacement in the node number 13 are obtained as follows:

Table B.2: Values of displacement coefficient in the node number 13.

$$\begin{aligned} A_{20} &= -0.6190\ mm \\ A_{22} &= -0.2970\ mm \\ A_{31} &= -0.1310\ mm \\ A_{33} &= 3.6766 \times 10^{-3}\ mm \\ A_{40} &= 2.8357 \times 10^{-3}\ mm \\ A_{42} &= 1.6887 \times 10^{-3}\ mm \\ A_{44} &= -4.7029 \times 10^{-5}\ mm \end{aligned}$$

Substituting the values of the coefficients listed in Table B.2 with $\theta = 30°$ and $\rho = 1$ into Eq.(2.44), the displacement at node number 13 is determined: $\omega(1, 30°) = -0.877mm$ (see the row 13 and column 2 in Table 4.3).

B.2 Calculation of Forces

The forces and deflections are related through Eqs.(3.35) and (3.36) which are expressed as Fourier series in Chapter 3. The force components in the Fourier series are associated with the coefficients of the deflection function given by Eq.(2.44) in Chapter 2. The mechanical properties of the lap plate are rewritten as follows:

Table B.3: Mechanical properties of the lap

Thickness of lap (h)	5 mm
Young's modulus (E)	90000 MPa
Poisson's ratio (ν)	0.25

We substitute the data listed in Table B.2 and Table B.3 into Eqs.(3.37), (3.38) and (3.39) to obtain the force components. Then the forces are calculated by Eqs.(3.35) and (3.36). We note that the forces are presented in per unit length; thus the results of the force obtained from Eqs(3.35) and (3.36) must be multiplied with the corresponding arc length between the two nodes in the lap

edge. Therefore, we obtain the results listed in Table B.4 which is the same as the values given in the 3rd row and 3rd and 4th columns in Table 4.2 as follows

Table B.4: Results of the calculated forces

No. of Load	Angle (degree)	Force (N)	Couple ($KN - mm$)
3	30	133.5682	-2.1448$\times 10^5$

VITA

Surname: Kang Given Names: Yan

Place of Birth: Beijing, China Date of Birth: Feb. 6, 1957

Educational Institutions Attended:

University of Victoria	1988 to 1990
Xian Institute of Technology	1978 to 1982

Degrees Awarded:

B.Sc.	Xian Institute of Technology	1982
M.A.Sc.	University of Victoria	1990

Publications:

1. Yan Kang, D.Y.He et al.,"Appl.of Computer-generated Hologram for testing Convex Aspheric Surfaces", ACTA METROLOGICAL SINICA, 7, 1986, P.30

2. Yan Kang, X.H.Shen, "Measuring Techniques for Complex-surface",OPTICAL ENGINEERING,1,19878, P.10

PARTIAL COPYRIGHT LICENSE

I hereby grant the right to lend my thesis to users of the University of Victoria Library, and to make single copies only for such users or in response to a request from the Library of any other university, or similar institution, on its behalf or for one of its users. I further agree that permission for extensive copying if this thesis for scholarly purposes may be granted by me or a member of the University designated by me. It is understood that copying or publication of this thesis for financial gain shall not be allowed without my written permission.

Title of Thesis: Figuring High Aspheric Mirrors by Elastic Deformation Method.

Author [redacted]
(Signature)

Yan Kang
(Name in Block Letters)

Jan 19, 1991
(Date)